Master's Thesis

Master in Telecommunication Engineering

Platinum microelectrodes fabricated on flexible substrate by inkjet Printing for pH sensing.

Miguel Zea

Director: Dr. Gemma Gabriel Buguña

Instituto de Microelectrònica de Barcelona (IMB-CNM CSIC)

Supervisor: Dr. Eloi Ramon Garcia

Electronic Department

Escola Tècnica Superior d'Enginyeria (ETSE)
Universitat Autònoma de Barcelona (UAB)

July 2016

El sotasignant, Dr. Gemma Gabriel Buguña i *Dr. Eloi Ramon Garcia*, Professor de l'Escola Tècnica Superior d'Enginyeria (ETSE) de la Universitat Autònoma de Barcelona (UAB),

CERTIFICA:

Que el projecte presentat en aquesta memòria de Treball Final de Master ha estat realitzat sota la seva direcció per l'alumne *Miguel Zea*.

I, perquè consti a tots els efectes, signa el present certificat.

Bellaterra, *07 de juliol de 2016* .

Signatura: *Dr. Gemma Gabriel Buguña* *Dr. Eloi Ramon Garcia*

“To Gemma, Ana , Eloi and Laura that unconditionally, have supported me along the way”

Barcelona, July 2016

Resum:

La impressió per injecció de tinta és una tecnologia emergent i de vanguardia en l'àrea de fabricació de biosensors. L'objectiu d'aquesta tesis és replicar mitjançant la impressió per injecció de tinta un sensor de pH prèviament fabricat per processos microelectrònics estàndards. Al present treball es demostra el potencial de la tecnologia de impressió per injecció per fabricar un AEIROF microelèctrode de platí en un rang de dimensions micromètriques per al sensat de pH, en substrats plàstics i flexibles. Es detalla pas a pas l'anàlisi, preparació, fabricació i caracterització necessaris per obtenir sensors de pH basats en AEIROF Pt mitjançant la impressió per injecció i tècniques de electrodeposició. El sensor de pH ha estat desenvolupat amb tintes de baix curat de Pt, Ag i SU8. Tres dimensions diferents d'elèctrodes han sigut caracteritzats. Els elèctrodes presenten una resposta electroquímica esperada. Aquest estudi també contempla la integració de una pseudo-referència de Ag/AgCl impresa. El sensor de pH mostra una resposta lineal super-Nerstiana en un rang de pH entre 1 i 11, amb una sensibilitat mitja de 0.065 V/pH i un temps de resposta inferior a 1 segon. Amb l'ús del a referencia integrada, el rang de mesura es limita entre 3 a 10 dècades de pH. Els sensors micromètrics presentats en aquest treball poden ser utilitzats en aplicacions que requereixin sensors d'un sol ús, per anàlisi ràpids i volums de mostres petits en sistemes portàtils per fer mesures in-situ. Totes aquestes característiques fan que aquest sensor tingui un especial interès a l'àrea de les aplicacions biomèdiques.

Resumen:

La impresión por inyección de tinta es una tecnología emergente y de vanguardia en el área de la fabricación de biosensores. El objetivo de esta tesis es replicar mediante la impresión por inyección de tinta un sensor de pH previamente fabricado por procesos microelectrónicos estándares. En el presente trabajo se demuestra el potencial de la tecnología de impresión por inyección para fabricar un AEIROF microelectrodo de platino en un rango de dimensiones micrométricas para el sensato de pH, en sustratos plásticos y flexibles. Se detalla paso a paso el análisis, preparación, fabricación y caracterización necesarios para obtener sensores de pH basados en AEIROF Pt mediante la impresión por inyección y técnicas de electrodeposición. El sensor de pH ha sido desarrollado con tintas de bajo curado de Pt, Ag y SU8. Tres dimensiones diferentes de electrodos han sido caracterizadas. Los electrodos presentan una respuesta electroquímica esperada. Este estudio también contempla la integración de una pseudo-referencia de Ag / AgCl impresa. El sensor de pH muestra una respuesta lineal super-Nerstiana en un rango de pH entre 1 y 11, con una sensibilidad media de 0.065 V/pH y un tiempo de respuesta inferior a 1 segundo. Con el uso de la referencia integrada, el rango de medición se limita entre 3 a 10 décadas de pH. Los sensores micrométricos presentados en este trabajo pueden ser utilizados en aplicaciones que requieran sensores de un solo uso, para análisis rápidos y volúmenes de muestras pequeños en sistemas portátiles para hacer medidas in-situ. Todas estas características hacen que este sensor tenga un especial interés en el área de las aplicaciones biomédicas.

Summary:

Inkjet printing technology is emerging at the forefront of biosensor fabrication technologies. This Master Thesis aims to replicate with Inkjet Printing technology a previously pH sensor fabricated with standard microelectronics processes. In this work it is demonstrated the potential of Inkjet printing Technology to achieve the fabrication of an Electrochemical growth Iridium Oxide Films (AEIROF) modified platinum microelectrode with feature sizes in the micrometer range for pH measurements on a flexible, plastic substrate. It is detailed step by step analysis, preparation, fabrication and set-up needed to obtain pH sensors based on AEIROF platinium by Inkjet and electrochemical deposition. The pH sensor was developed with Pt, Ag and SU8 low curing inks. Three different dimensions of electrodes are characterized. Electrodes exhibit the expected response in terms of electrochemical response. This study also integrates an Ag/AgCl printed pseudo-reference. The AEIROF pH sensor exhibited a linear super-Nerstian response between pH 1 and 11, with averaged slope of 0.065 V/pH and response speed of less than a second. With the pRE response is limited between pH 3 and 10. However the presented printed sensors allow their used in applications. All the results make the presented manufacturing approach interesting for a wide range of sensor applications. The micrometric dimensions of the presented printed sensors allow their used in applications that requires disposable devices, low analysis time, sample volumes and portability for in-situ analysis. All these characteristics make this pH sensor of interest especially in the biomedical applications field.

Contents

1 Introduction **3**

1.1 Introduction to Inkjet Printing 4

1.2 State of art pH sensors 8

1.3 State of art of printed pH sensors 10

2 Objectives **11**

3 Materials and Methods **13**

3.1 Chemical reagents 13

3.2 Inks for Inkjet 13

3.3 Substrates 14

3.4 Equipments 14

3.5 Methodology 15

3.5.1 Sheet resistance 15

3.5.2 Profilometry 15

3.5.3 Drop Spacing 16

3.5.4 Electrochemical impedance 16

3.5.5 Cyclic voltammetry 17

3.5.6 Electrochemical activation 17

3.5.7 Electrodeposition of AEIROF 17

3.5.8 Ag pseudo-reference Chlorination 18

3.5.9 pH measurement and sensor calibration 18

4 Results **19**

4.1 Pt ink print optimization 19

4.1.1 Waveform optimization 19

4.1.2 Drop spacing optimization 20

4.1.3 Sheet resistance 22
4.1.4 Pt Ink characterization 23
4.2 SU8 ink print optimization as passivation 26
4.3 Ag ink print optimization for pseudo-reference 27
4.4 Microelectrodes fabrication 28
4.4.1 Passivation strategy 30
4.4.2 Pseudo reference performance 31
4.5 Electrochemical characterization of Pt microelectrodes 32
4.5.1 Impedance measurement 32
4.5.2 Cyclic voltammetry 35
4.5.3 Electrochemical Activation 40
4.6 Electrochemical characterization of AEIROF microelectrodes 43
4.7 pH sensor calibration 44

5 Conclusions **46**

Chapter 1

Introduction

Inkjet printing technology is emerging at the forefront of biosensor fabrication technologies. Parallel advances in both ink chemistry and printers have led to a biosensor manufacturing approach that is simple, rapid, flexible, with high resolution, low cost, efficient for mass production, and extends the capabilities of devices beyond other manufacturing technologies.

This Master Thesis was carried out at in the Institute of Microelectronics of Barcelona (IMB-CNM CSIC). The research activities of IMB-CNM are dedicated to Micro/Nano Integrated Systems: miniaturized electronic systems which include sensing and/or actuating capabilities in addition to electronic information processing, power management and external interfaces. The work of this Master Thesis was performed with Biomedical Applications Group (GAB). The research activities of the GAB takes advantage of the technological capacities available at the Clean Room of the IMB-CNM in order to provide novel solutions to different biomedical applications. The group is interested in three major topics: Biosensors, Neuroscience and Organ-on-a-chip. One year ago, the GAB began to investigate in the use of Inkjet printing technolog for the fabrication of biosensors. Microtechnology-based smart devices for online monitoring of biologic structures such as biofilms or culture cells are being fabricated by the GAB. In particular, biosensors to measure the cell adhesion by means of impedance measurement, pH, dissolved oxygen and ions (Na^+, K^+, Ca^{2+}) concentration are now being developed [1][2][3] by traditional fabrication techniques (Photo-lithography). Currently the main GAB interest is focused in the development of the manufacturing processes to set-up Inkjet technology to produce these biosensors with Inkjet printing technologies.

This Master Thesis aims to replicate a previously pH sensor fabricated with standard microelectronics processes by GAB [3], now with Inkjet printing Technology. It will be detailed step by step analysis, preparation, fabrication and the set-up needed to obtain pH sensors based on electrochemical growth of iridium oxide films (AEIROF) platinium by Inkjet and Electrochemical deposition.

This chapter has the aim to show to the reader some key information to understand the rest of the text. A brief introduction to Inkjet printing will be done, in which the importance and the advantages of this technology are shown. After this, the state of art of pH sensors, as well as some examples of pH sensors made by different printing techniques will be done.

1.1 Introduction to Inkjet Printing

Inkjet printing is a contact less, an accurate and reproducible preparation technique, which relies on the formation of individual droplets that are ejected from a nozzle that allows the maskless deposition of different functional materials on rigid and flexible substrates. It is based on digitally controlled ejection of fluid drops from a small aperture, named nozzle, directly to a pre-specified position [4]. The original idea of the Inkjet printing technology is attributed to Lord Rayleigh in 1878, who proposed a liquid jet of constant radius able to fall vertically under gravity [5]. As the liquid length increases and reaches a critical value, the jet loses its cylindrical shape and decomposes into a stream of droplets (Figure 1.1) for this reason is necessary an accurate control of printing parameters. This has led to two main modes of operation, continuous and drop-on-demand (DOD) printing technologies.

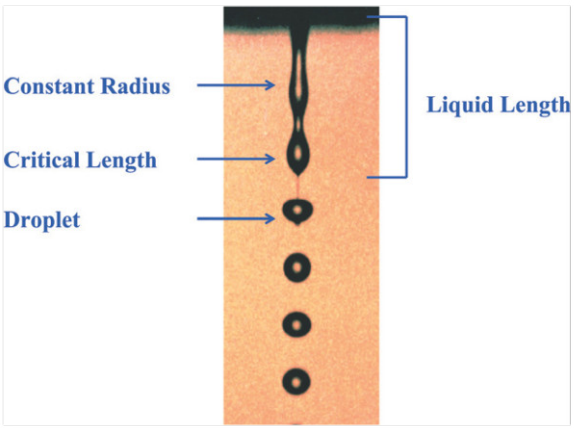

Figure 1.1: Lord Rayleigh's idea of instability of jets. From [6]. Copyright 2001 Society of Photo Optical Instrumentation Engineers.

Inkjet printers

In a continuous Inkjet nozzle (Figure1.2), the creation of the ink stream is constant. A piezoelectric (PZT) crystal creates an acoustic wave as it vibrates within the gunbody and causes the stream of liquid to break into droplets. The ink droplets are subjected to an electrostatic field created by a charging electrode. The charged droplets pass through another electrostatic field and are deflected

by electrostatic deflection plates to print on the substrate, allowed to undeflected droplets goes into a gutter for recirculation. Only a small fraction of the droplets is used to print, the majority are being recycled.

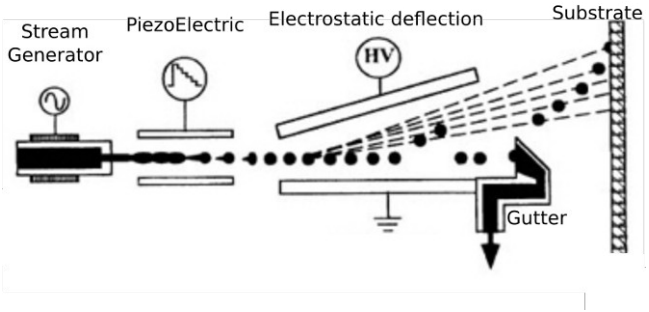

Figure 1.2: Drop formation and continuous ejection method scheme of an Inkjet printing equipment

The DOD inkjet printer ejects the ink only when it is required. The DOD eliminates the complex droplet charging, deflection and recycling system, and allows higher placement accuracy. The DOD printer relies on a pressure pulse created to form ink droplets. The method used to generate this pressure pulse defines the primary subclasses of the DOD printer, called thermal [7], PZT [8]. The work of this Master Thesis has been done with a DOD PZT printer.

DOD PZT works applying a voltage to an ink-filled chamber through a PZT transducer. The PZT material changes its shape with voltage, generating a pressure pulse in the fluid, which forces a droplet of ink from the nozzle [4]. Piezoelectric Inkjet allows a wider variety of inks than the thermal one as there is no requirement for a volatile component. However, the printheads are more expensive due to the use of PZT material (usually PZT is lead zirconium titanate). In Figure 1.3 it is shown an scheme of the drop formation in a PZT DOD printer.

Inkjet printing inks.

In order to inkjet-print a sensor, at least two types of inks/materials are needed: conductor and insulator ink. The most commonly used conductor ink is a nanoparticle-based where metallic particles are in the nanometer range (5-100 nm). Particles are encapsulated with a thin protective organic shell and dispersed in a liquid solvent. After printing on a substrate, a heating/sintering step is used to firstly evaporate the solvent, followed by the disassociation of the encapsulant/dispersant, and finally to melt the metallic nanoparticles resulting in a metal thin film. The process [11][12] is depicted in Figure 1.4. Therefore, nanoparticle-based inks are promising candidates for producing electrodes and interconnections for printed devices. The required temperature for the sintering of the

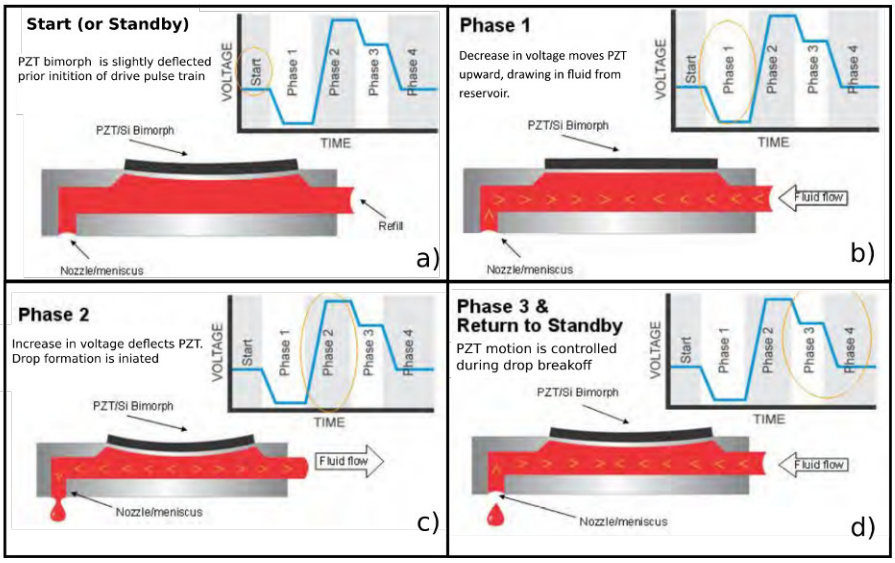

Figure 1.3: a), b), c) and d) show the steps for ejecting ink as movements of PZT applying voltage to printer. Image from [9]

nanoparticles is determined by the size of the particles and the encapsulant/dispersant. The melting point of metal nanoparticles is significantly reduced (relative to the bulk melting point) due to a high surface-to-volume ratio. E.g. butane-thiol encapsulated gold nanoparticles with 1.5 nm size have been demonstrated to sinter at a temperature as low as 120 ^{o}C [13]. For this work it has been used a novel commercial platinum ink, specially formulated for low curing temperatures (lower than 180 ^{o}C). So, this ink allows the use of paper or plastic substrates.

For the insulator ink, organic dielectric materials are more widespread than their inorganic counterparts. The most commonly used polymer dielectric is Poly(4-vinylphenol) (PVP) that can be dissolved in alcohol based solvents for inkjetting. Several crosslinking agents are typically used to chemically crosslink the PVP into an electrical insulator. However, in this Master Thesis it will be used a SU8 based ink (Microchem PriElex) due to its high chemical resistance, excellent thermal stability and optical transparency due to the previous experience in the GAB using this material as dielectric. The advantage of inkjetting a polymer comparing to a nanoparticle ink is that the viscosity can be adjusted directly by changing the polymer concentration in the solvent.

Waveform generation for ink ejection

In Figure 1.3 there is the waveform representation that is used to control the PZT by voltage. The typical basic waveform is divided into four segments (Figure 1.5) [9]. Each segment has three properties: duration (time), level and slew rate of the applied potential.

The level values, which resemble a percentage of the voltage in segment one and two have the most

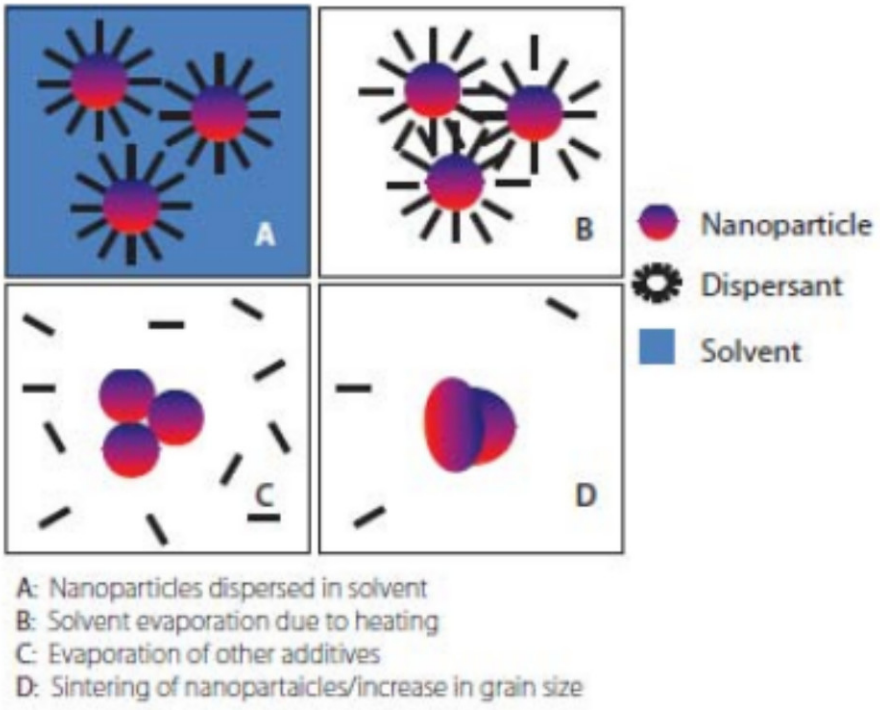

Figure 1.4: Schematic of a sintering process of nanoparticle inks: a) before heating, b) Slvent evaporates and start degradation by heat, c) sintering start, and d) sintering finish [12]

impact on the jetting process. Changing the duration of segment one and slew rate and/or duration of segment two has a strong influence on drop formation. The applied voltage relates directly to the volume of the pumping chamber. Faster changes in voltage change the volume faster, bigger changes in voltage cause bigger volume changes. The slew rate determines how fast the volume changes.

Waveform generation is highly dependent to the ink properties, and also its ejection. Ink viscosity, density and surface tension are crucial for Inkjet printing [10]. In general, viscosity determines the velocity and the amount of the fluid ejected and it should be below 20 mPas. Surface tension determines the shape of the droplet and in order to obtain spheroids it should range from 30 mN/m to 350 mN/m [10]. Consequently inks need to be prepared taking into account this values or near by. Usually additives are needed in order to adjust the ink properties, producing changes in the ink conductivity, the adherence to substrate, and the ink sintering temperature. For these reasons, ink characterization must be done before carry out any Inkjet printing process.

Summarizing, Inkjet printing is extremely versatile for prototyping, thus enabling rapid manufacturing via high pattern precision and resolution thanks to DOD. Main advantages of the technology are non contact, material efficient, reproducible, editable processing and low-cost. One of the most interesting Inkjet printing applications is the fabrication of sensors and biosensors.

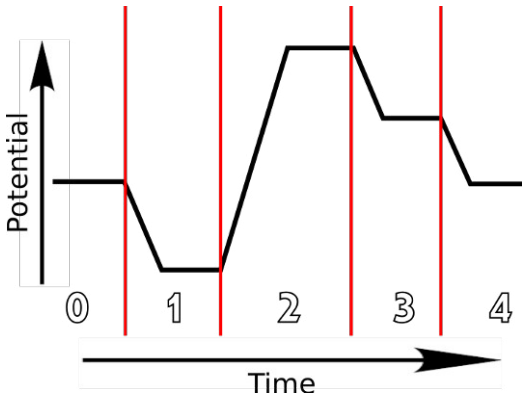

Figure 1.5: Basic waveform for Ink ejection

1.2 State of art pH sensors

A pH sensor is an instrument that measures the hydrogen ion concentration (H^+) in a solution, giving information related to the acidity or alkalinity of the medium. The pH sensor measures the difference in electrical potential between an electrode and the solution and also uses a reference electrode. The pH sensors are widely used in chemical and biological applications such as food quality, blood pH measurements and laboratory pH measurements amongst others.

The most common pH sensor is the glass electrode. A potential is developed at the pH-sensitive glass membrane as a result of differences in hydrogen ion activity in the sample and a standard solution contained within the electrode. This potential measured about the potential of the reference electrode gives a voltage that is expressed as pH. Instrumentation for pH measurement is among the most widely used process measurement devices. Rugged electrode systems and highly reliable electronic circuits have been developed for this use [14].

In addition to the glass pH electrode specific for hydrogen ions, exist alternative pH detection sensors:

- pH indicator: it is a halochromic chemical compound added in small amounts to a solution so the pH of the solution can be visually determined. Hence, a pH indicator is a chemical detector for hydronium ions (H_3O^+) or hydrogen ions (H^+) in the Arrhenius model. Normally, the indicator causes the color of the solution to change depending on the pH [15].

- Hydrogen-Electrode Method: uses a hydrogen electrode made by adding platinum black to platinum wire or a platinum plate. It is immersed in the test solution with a silver chloride electrode, then an electric charge is applied to the solution and the solution is saturated with hydrogen gas. The potential is measured between both electrodes. The measured potential is correlated with the pH of the solution.

- Hydrogen-Electrode Method: uses a hydrogen electrode made by adding platinum black to platinum wire or a platinum plate. It is immersed in the test solution with a silver chloride electrode; then an electric charge is applied to the solution and the solution is saturated with hydrogen gas. The potential is measured between both electrodes and correlated with the pH of the solution.

- Quinhydrone-Electrode Method: When quinhydrone is added to a solution, it separates into hydroquinone and quinone. Because quinone's solubility varies depending on the pH value of the solution, pH can be determined from the voltage between a platinum and reference electrode.

- Antimony-Electrode Method: This method involves immersing the tip of a polished antimony rod into a test solution, also immersing a reference electrode, and measuring pH from the difference in potential between them.

- Semiconductor sensor methods: It is an ion sensitive field-effect transistor (ISFET), that is used for measuring ion concentrations in solution; when the ion concentration changes, the current through the transistor will change accordingly. Here, the solution is used as the gate electrode. A voltage between substrate and oxide surfaces arises due to an ion sheath [17]. [16].

Moreover more methods have been proposed as; optical fiber pH sensors [18], hydrogel film pH sensors [19], and solid-state pH sensors [20] . Also pH sensor on flexible substrate by standard photolithography and lift-off processes are reported [21].

For this work, It is important to mention also the use of iridium oxide. This material has a particular interest due its various interesting properties that have attracted the attention of many researchers over the last four decades. Many studies have been performed, targeting the application of iridium oxide films as electrocatalysts [31], chemical sensors [32], neurostimulators [33] and super-capacitors [34]. Iridium oxide films for sensing are categorized in metal oxide/metal sensors. These are based on an equilibrium between oxides, in which the metal has different oxidation states. Iridium oxide pH sensors are based on the existence of Ir(III), Ir(IV) and Ir(V) oxides [39].

Metal oxide/metal sensors should satisfy several criteria to be useful as pH transducers, such as stability over a wide pH range, electrical conductivity, and ability to come into equilibrium with the solution measured without significant dissolution [35]. Iridium oxide films (IROF) present some advantages compared with other materials (such as antimony or palladium), including response over a wider pH range, low impedance, fast response even in non-aqueous solutions, and excellent biocompatibility [36]. IROF can be produced by numerous methods, including sol–gel processes, thermal decomposition of iridium salts, melt oxidation, reactive sputtering (SIROF), electrochemical oxida-

tion (AIROF), or electrochemical growth (AEIROF), that generate products of different behavior and pH response [37]. For this Master Thesis, AEIROF method was used for the validation of our microelectrode as the pH sensor.

1.3 State of art of printed pH sensors

Related with this work, it has been previoulsy reported the fabrication of other pH sensors with several printed electronic technologies. Related with printed electronics the most important techniques are screen printing, flexography, gravure, offset lithography, and Inkjet.

There is no an entirely Inkjet pH sensor reported at the moment. However, pH sensors are reported by partially Inkjet and screen printing. For screen printing Koncki et al., designed a flexible, fully screen-printed, disposable pH sensor based on ruthenium dioxide by the application of a thick-film. The electrodes allow fast measurements, with excellent sensitivity (51 mV/pH), in acidic and neutral solutions [40]. Furthermore, Dimitrios K. Kampouris reported also a screen-printed electrochemical platforms for pH sensing [42]. These ones combine the pH sensitive phenanthraquinone moiety which has a Nernstian potential shift with pH, and an internal reference of insensitive pH dimethylferrocene.

Cheng-En Lue reported a pH sensing reliability of flexible ITO/PET electrodes on EGFETs prepared by a roll-to-roll process [43]. This sensor is an electrode of extended gate field effect transistors (EGFETs). The sensor has a sensitivity of 50.1 mV/pH between pH 2 to pH 12, and it was deposited on PET.

Yihen Qin reported Inkjet-printed bifunctional carbon nanotubes for pH sensing [44]. This sensor can be understood partially fabricated with Inkjet because it consists of an electrode of carbon nanotubes deposited by Inkjet. However the pads and the electrical contacts are manually painted with silver paste and a polydimethylsiloxane (PDMS) layer was manually dropped on top of the painted Ag for passivation. The sensor has a sensitive of 48.1 mV/pH from pH 3 to pH 11.

pH sensors with both printed reference and working electrodes on one substrate by printed electronics are reported in the literature [41], due the need to fabricated a miniaturized portable sensor device. In this sensor Screen printed iridium (IV) oxide electrodes have been manufactured, as well as ruthenium (IV) oxide ones. For the reference they used a silver/silver chloride electrode.

Chapter 2

Objectives

Specifically, the aim of this Master Thesis is to demonstrate the potential of Inkjet printing technology to achieve the fabrication of an AEIROF modified platinum microelectrode with feature sizes in the micrometer range for pH measurements on a flexible, plastic substrate. Also, the integration of a modified Ag/AgCl printed microelectrode for a miniaturized potentiometric pH sensor is contempled at the end of the work.

As the desired materials for printing these pH sensors are low cost plastic substrates, it was used a novel Pt ink formulation for low curing temperatures. The printing optimization of this ink was completely done in this work.

This pH sensor consists of a working electrode (WE) of platinum (Pt) and a pseudo-reference electrode (pRE) of silver/silver chloride (Ag/AgCl), all printed on a flexible substrate with feature sizes in the micrometer range. Moreover SU8 ink is used as dielectric material to print passivation patterns on tracks and electrodes to precisely define the active area of the electrodes. To accomplish this work, different sub-objectives were defined:

- Novel low curing Pt ink characterization.
- SU8 ink, Ag ink optimization.
- Microelectrodes design and fabrication in different sizes.
- Pt microelectrode electrochemical characterization.
- Pt microelectrode surface modification with AEIROF deposition for pH measurement and its electrochemical characterization
- Ag/AgCl pRE microelectrode integration.

Novel low curing Pt ink characterization.

Fraunhofer IKTS has recently developed a novel Pt ink formulation for Inkjet printing at low curing temperatures. As GAB did not have experience with this ink, great efforts have been done with its characterization and optimization . Basically the work have been focused in the waveform optimization, the drop spacing characterization and the sheet resistance measurements. And a morphologic studies of SEM, AFM and optical microscope were carried out.

SU8 ink, Ag ink optimization.

SU8 and Ag ink are already in use at GAB to fabricated Inkjet devices. They are needed for passive tracks and also a reference electrode for our sensor. SU8 and Ag inks need to be optimized and restudied. (waveform, drop spacing and sheet resistance)

Microelectrodes design and fabrication in different sizes.

For the electrodes fabrication: it is necessary to design them, overcome the technological challenges of Inkjet and make them reproducible. The device is designed to be compatible with a Zero Insertion Force (ZIF) to make it easy to handle. The different fabrication steps will be optimized.

Pt microelectrode electrochemical characterization.

For the validation of the microelectrodes, an electrochemical characterization is needed. The characterization will be basically made with impedance and cyclic voltammetry measurement.

Pt microelectrode surface modification with AEIROF deposition for pH measurement and its electrochemical characterization.

To detect pH AEIROF layer must be electrodeposited on the electrodes. In order to validate their correct deposition, impedance and cyclic voltammetry measurement are done. Then electrodes need to be calibrated in different pH solutions by open circuit potential test to ensure its correct operation.

Ag/AgCl pRE microelectrode integration.

A printed Ag microelectrode will be chloronized to fabricate Ag/AgCl pseudo-reference electrode improved potential stability to enable a potentiometric measurement with a completely minaturized pH sensor.

Chapter 3

Materials and Methods

Next sections shows material and methods needed to reach objectives.

3.1 Chemical reagents

Ethanol (LC/MS grade), potassium nitrate (KNO_3), Potassium hexacyanoferrate(III) ($K_3[Fe(CN)_6$) and potassium hexacyanoferrate(II) trihydrate ($K_4[Fe(CN)_6]$) (all from Sigma-Aldrich, Spain) were used for surface cleaning, activation and characterization of the printed sensors. Hydrochloric acid (HCl)(0.1 M) was electrochemically applied for the chlorination of the printed silver layers, and potassium chloride (KCl) for testing the open circuit potential of the pRE (both from Sigma-Aldrich, Spain).

Iridium trichloride trihydrate ($IrCl_3 * 3H_2O, 99.9\%$), oxalic acid ($H_2C_2O_4 * H_2O, 99\%$), potassium carbonate $(K_2CO_3, 99\%)$ were used for the development of the pH sensor.

3.2 Inks for Inkjet

For the development of the pH sensor, it has been used three inks. A platinum nanoparticle ink (Pt-LT-20 from Fraunhofer IKTS, Germany) was employed for printing the working electrode. The ink shows drop-on-demand (DoD) inkjet compatible specifications with a solid content of 20 wt%., a viscosity of 10.50 mPas (100/sec at 22ºC), a density of 1.25 g/mL (at 22ºC) a surface tension of 31.70 mN/m (at 22 ºC) and a mean particle size of about 40 nm. Pt sintering temperature is 170 - 240 ºC.

A silver nanoparticle ink (DGP-40LT-15C from ANP, Korea) was used for printing the pRE electrode. The ink shows drop-on-demand (DoD) inkjet compatible specifications with a solid content of 30-35 wt%., a viscosity of 10-18 mPas (at 25 ºC), a density of 1.45 g/mL (at 25ºC) a surface tension

of 35-40 mN/m (at 25 ^{o}C) and a mean particle size of about $<$50 nm. Ag sintering temperature is 100-150 ^{o}C.

The passivation of the electrodes was done using the SU8 ink (PriElex from MicroChem, USA). SU8 has a viscosity of 9-12 mPas (at 25 ^{o}C), a density of 1.0.38 g/mL (at 25^{o}C) and a surface tension of 27-32 mN/m (at 25 ^{o}C). SU8 is cured by ultraviolet light (UV)

3.3 Substrates

Teonex PEN films (Q65HA DuPont Teijin Films) with a thickness of 125 μm and a surface pre-treatment for improved adhesion and Kapton polyimide film (500HN DuPont Teijin Films) with a thickness of 127 μm were selected as substrate.

The surface energy of substrates was measured. Obtaining that PEN film has a surface energy of 38.3 mN/m and Kapton polyimide film has 50 mN/m. Moreover, the maximum afforded temperature of PEN is 200 ^{o}C and for the Kapton is 360 ^{o}C.

3.4 Equipments

A PZT Dimatix Material Printer (DMP 2831 from FUJIFILM Dimatix, Inc., USA) was employed for the inkjet printing of the three inks on the Kapton substrate. The printer was equipped with a fillable 10 pL nominal drop volume printheads having 16 nozzles each with a diameter of 21.5μm. Printing patterns were made using Electronic Design Automation (EDA) layout software and imported with the Dimatix Bitmap editor software. The printer vacuum plate where the substrate is placed is temperature controllable. The printing processes were carried out in a standard laboratory environment in ambient condition, without non-particulate filtered enclosure systems and without control of temperature or humidity to determine the extent to which the sensor devices could be manufactured on an industrial-scale printing system.

Scanning Electron Microscopy (SEM) (Auriga-40 from Carl Zeiss) was used to study the morphology of each printed layer. An Atomic Force Microscope (AFM) (Dimension 3100 head from Veeco) was employed to analyze the topography and roughness of the printed layers and a profilometer (Dektak 150 from Veeco) was used for the thickness measurement of the layers. The sheet resistance of each conductive layer was determined with a Hewlett Packard HP4155 Semiconductor Parameter Analyzer connected to a manual probe station Karlsuss PA200.

Electrodes impedance was measured with SI1287 Electrochemical Interface and SI1260 Impedance/Gain-Phase Analyzer (Solartron, United Kingdom). The electrochemical characterization and calibration

of the sensors were performed with an 8-channel potentiostat 1030A Electrochemical Analyzer (CH Instruments, USA). Control experiments were performed using a commercial Ag/AgCl (3 M KCl) electrode as reference and a platinum ring electrode as counter electrode, (both from Metrohm, Germany). Printed sensors were calibrated in a buffer PBS solution against a pH meter (GLP22 from Crison, Spain) pH meter probe.

3.5 Methodology

3.5.1 Sheet resistance

The sheet resistance measurements were done on the four-point probe table. It consists of four points being placed at the corners of the samples following the Van der Pauw technique (Figure 3.1). Data was obtained by the Semiconductor Parameter Analyzer. [28]

For the resistance study of the printed material, two tests were performed.

1. Nine single layers squares of 4x4mm were printed. Then, three groups of three squares were placed on the hot plate, at different temperatures each group (150, 180 and 200°C) and each square at a different time (15, 30 and 60 mins). To find the sheet resistance in function of temperature and time for sintering.

2. Four squares were printed with several layers from 1 to 4 layers. Then they were placed on hot plate at selected sintering temperature and time found in the first test (30 min at 180°C)

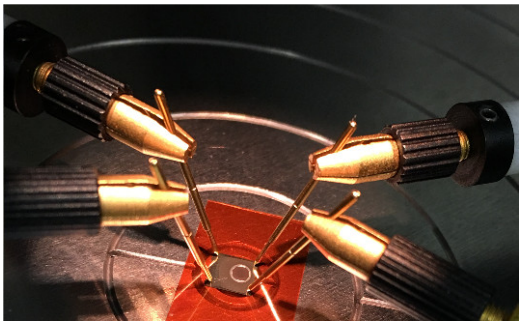

Figure 3.1: Four-point probe measurement

3.5.2 Profilometry

Profilometry study was done in order to quantify roughness and thickness of printed materials. A profilometer works thereby, a diamond stylus is moved vertically in contact with a sample and then moved laterally across the sample for a specified distance and specified contact force. A profilometer can measure small surface variations in vertical stylus displacement as a function of position. A

typical profilometer can measure small vertical features ranging in height from 10 nanometers to 1 millimeters.

3.5.3 Drop Spacing

The Drop Spacing (DS) is the center to center distance in X and Y of two consecutive drops. For the Dimatix the DS is adjustable between 5 and 254 μ m in five-micron increments. For example, with a DS50 (DS of 50 μ m), the pattern generator places drops 50 μ m apart in X and 50 μ m apart in Y to fill in the pattern. So, for a 100 μ m wide, 10 mm tall vertical line, the system places 3 drops in the X direction (one for the first edge, another at 50 μ m, and another at 100 μ m for the next edge) by 2,001 drops tall. The DS, therefore, determines resolution or density in the X direction and Y direction. The amount of jetted ink per area depends of the selected DS.

In order to know the DS necessary for printing a continuous line, a line pattern test design is used. It consists in an array of lines with different DS, as it is shown in the Figure 3.2. This array was analyzed in the profilometer to know the thickness and width of the ink with DS variation.

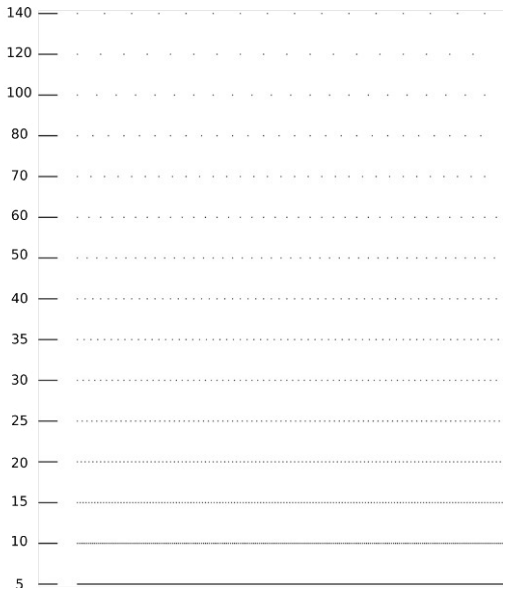

Figure 3.2: Line Pattern design

3.5.4 Electrochemical impedance

Two-electrode impedance measurements were conducted to characterize the electrode-electrolyte interface impedance versus to a platinum electrode (Radiometer Analytical). The electrical properties of the electrode-electrolyte interface were evaluated by comparing the impedance and phase shifts to the frequency in PBS (15.52 mS/cm) in the 10 Hz to 1 MHz frequency range.

3.5.5 Cyclic voltammetry

In a cyclic voltammetry (CV) experiment, the working electrode potential is ramped linearly versus time. Unlike in linear sweep voltammetry, in a CV experiment after the set potential is reached the working electrode's potential is ramped in the opposite direction to return to the initial potential. The current at the working electrode is plotted versus the applied voltage to give the cyclic voltammogram trace. CV is a commonly used technique for comparing and studying the behavior of the electrodes. The electrochemical reversible ferro(II)/ferri(III)-cyanide redox couple $[Fe(CN)_6]^{4-} \Longleftrightarrow [Fe(CN)_6]^{3-} + e^-$ was chosen for the CV experiments carried out.

3.5.6 Electrochemical activation

Following reported works [29], the application of a suitable potential waveform to clean the Inkjet printed electrodes was chosen. In particular, five pulses alternating between -2V and 0 V for 10 seconds in a KNO_3 electrolyte solution were performed. Subsequently, in order to verify the optimal activation response, cyclic voltammetry measurements in ferro/ferricyanide ($10^{-2}M$) at different scan rates were carried out.

3.5.7 Electrodeposition of AEIROF

The solution for the iridium oxide deposition is made from 0.2 mM of $IrCl_3 * 3H_2O$, 1 mM of $H_2C_2O_4 * 2H_2O$ and 5 mM of K_2CO_3 dissolved in a total amount of 50 ml deionized water. The materials are put in one by one, between each the solution is stirred for half an hour. Afterwards, the solution ages four days at 37 degrees Celsius.

AEIROF thin films were obtained by a dynamic potential sweep method consisting of 50 potential sweeps between open circuit potential (near 0.0 V) and 0.6 V at a scan rate of 10 mV/s. Under these conditions, the AEIROF thickness, measured with the aid of profilometer, was of 300 nm. No free particles or film cracks were observed by atomic force microscopy or scanning electron microscopy [3]. As it has been shown previously, this preparation method induces the formation of an Ir-oxohydroxide with reproducible stoichiometry and sponge-like quasiamorphous open structure (local rutile structure) as derived from X-ray diffraction and XPS (reproducible mixed-valence states). A detailed study of the structure and composition of the AEIROF produced has been published in a previous work [38]. Once prepared, the sensors were stored in PBS at room temperature.

3.5.8 Ag pseudo-reference Chlorination

To obtain a stable Ag/AgCl pseudo-reference electrode (pRE)[45] it is necessary to chlorinate the silver electrode. The chlorination is done with a cyclic voltammetry in 0.1M HCl, scanning the potential from 0 V to 0.2 V vs an external Ag/AgCl commercial reference electrode at 20 mV/s^{-1} Figure 3.3.

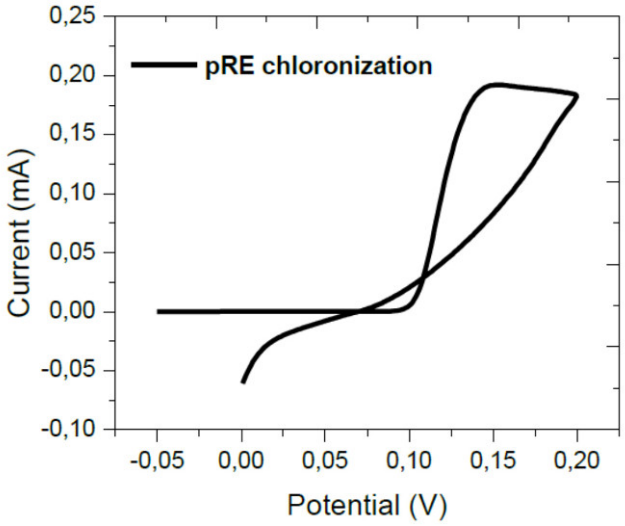

Figure 3.3: Cyclic voltammetry applied for the chlorinated process of the printed silver.

3.5.9 pH measurement and sensor calibration

Potentiometric pH measurements were carried out on a CH Instruments 1030A potentiostat by registering open circuit potential against either an external Ag/AgCl reference electrode and an internal ink Ag/AgCl pRE. For the calibration of the AEIROF pH sensor, the response was studied in terms of open circuit potential evolution over time in a pH range between 3 and 11. PBS was used as buffer solution and the pH was modified, under mechanical stirring, by serial addition of either NaOH or HCl. The solution pH was monitored in parallel using a GLP22 commercial pH-meter (CRISON) connected to a PC through a custom interface.

Chapter 4

Results

This section shows step by step inks printing optimization, microelectrodes fabrication, electrochemical respond of Pt electrodes, electrochemical respond of IrOx, pH sensor calibration with external reference and pH sensor calibration with internal pseudo reference (pRE).

The pH sensor of this master thesis consists of a Pt working electrode and Ag/AgCl pRe printed on a flexible plastic substrate. For the working electrode, Pt ink was selected due the need of electrodeposition of IrOx to Hydrogen ions detection. Ink selection is because has been demonstrated that adhesion of IrOx is better over Pt than other materials [3]. For pH sensing, the WE needs a reference electrode reason why a pRe electrode is integrated into the sensor. Also for passivation of electric pads a dielectric ink was used, for this work was SU8 ink.

4.1 Pt ink print optimization

As it is known the most important weakness of this technology remains in the ink properties because from this properties depend if it is a printable material or no. As it is described above, viscosity, surface tension and density are important features to allow a controlled printing. Moreover, flexible substrates have temperature limitations, limiting sintering temperatures. This is the main reason why it was selected this low curing Pt ink for the development of the pH sensor.

The platinum ink was bought at Fraunhofer; it is a new formulation that it has been not characterized. Reason why all the characterization was necessary.

4.1.1 Waveform optimization

The drop ejection behaviour of the inkjet nozzle was visually checked using the integrated dropwatcher camera in the Dimatix printer to ensure stable process conditions. The relative distribution

of deposited material across the printer geometry was controlled by adjusting parameters such as the printhead nozzle temperature, the jetting frequency, the jetting waveform and the maximum voltage applied to the printhead nozzles. For the generation of the waveform of Pt ink. It was considered that Pt ink has the same manufacturing (Fraunhofer) of a gold ink previously studied in the GAB [46]. Because of this, the waveform of gold ink was taken as a starting point. Different waveforms were developed to fine-tune the drop ejection of the Inkjet printheads, Finally the waveform and drop ejection optimized is shown in Figure 4.1.

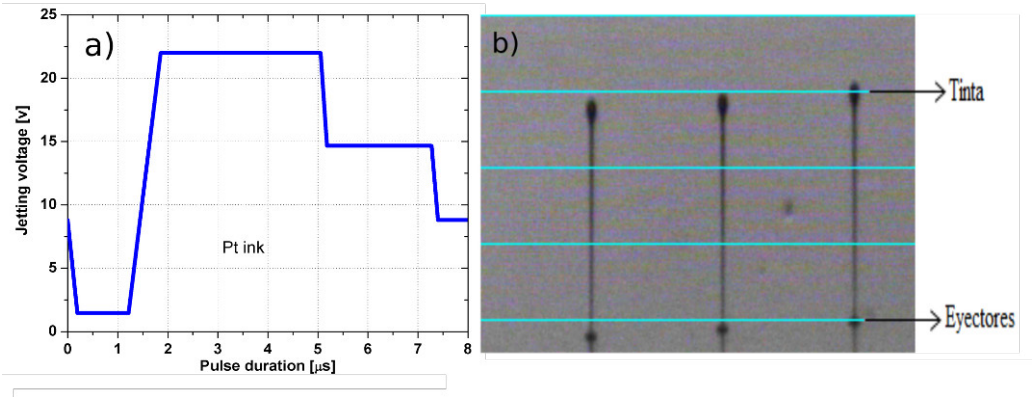

Figure 4.1: a) Waveform applied to the PZT of the printhead for the Pt ink ejection and b) Dropwatcher images of ejected droplets from the inkjet printhead

The Figure 4.1b) shows Pt drops with long fluid tails. However, the tails did not rupture creating satellite drops. Instead, the tails reach the leading droplet during the flight and merge with it prior the impact on the substrate. No separation ensure a high printing quality.

4.1.2 Drop spacing optimization

A dedicated test print pattern was developed using line pattern design (Figure 3.2) that allows the deposition of lines with different DS but with a fixed width of 1 px (pixel). Figure 4.2 shows the print pattern as well as the resulting line pattern for the Pt ink.

These printed patterns were deposited with a platen temperature of 25, 30, 40 and 60 °C Figure 4.3 shows the resulting width of each printed continuous line formation. We selected the DS taking into account the width and the thickness that we aimed to obtain for our sensor design with a continuous line formation. The line morphology strongly depends on the diameter of a single printed drop. For the Pt ink, the single drop diameter was determined to about 77 $\pm$ 2 μ m A DS of 25 μ m at 25 °C was selected for the line pattern which results in a line width of about 100 $\pm$ 7.9 μ m and a thickness of approximately 100 $\pm$ 20 nm.

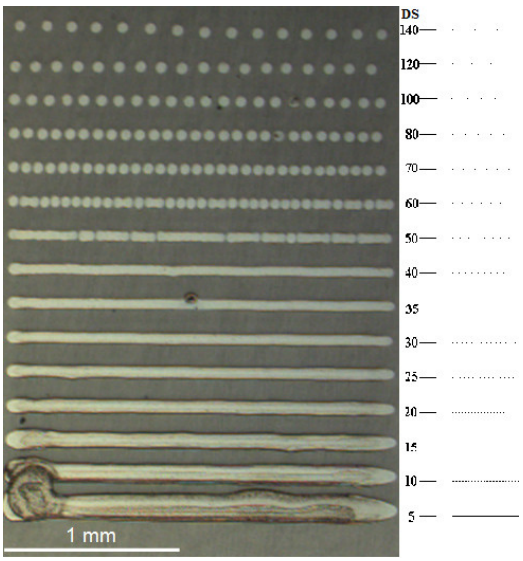

Figure 4.2: Line formation regimes depending on the drop spacing selected.

The Pt ink was printed using a DS of 25μ m This DS was found to be the optimum compromise between low line width (small feature size of the sensor device) and stable, continuous line formation without interruptions resulting in open electrical contacts. Finally, Pt print did a 25 ^{o}C because higher temperatures obstruct nozzles due ink drying on it.Finally, Pt print was did a 25 ^{o}C because higher temperatures obstruct nozzles due ink drying.

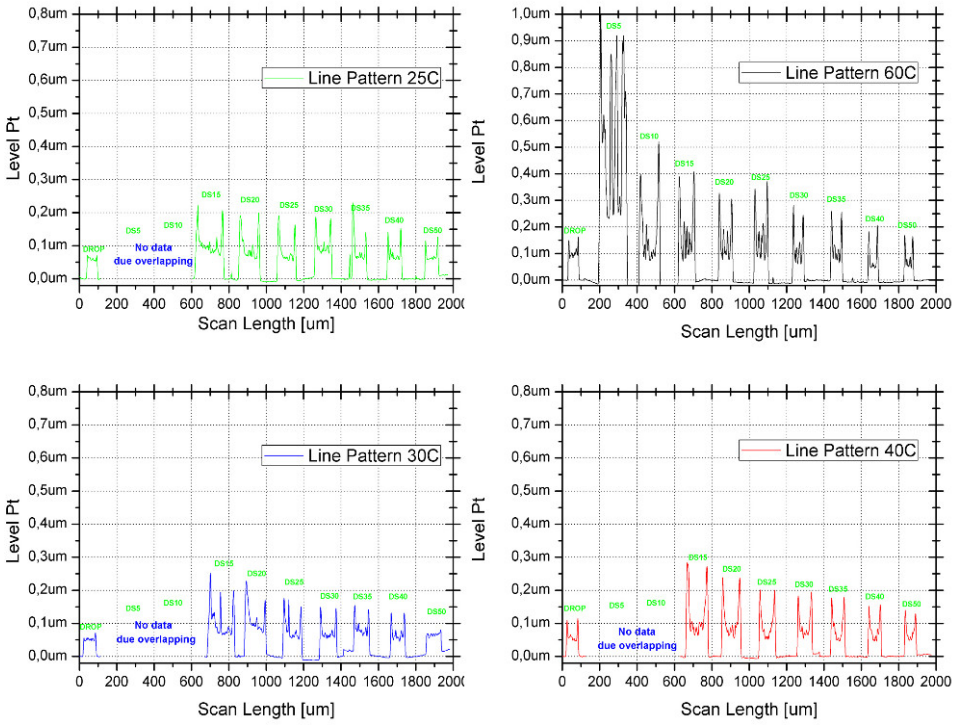

Figure 4.3: Printed lines at different drop spacing and different platen temperatures for Pt ink.

As it can be observed in Figure 4.3 at 25, 30 and 40^{o}C platen temperature lines of DS 5 μ m and

	1 Layer	2 Layers	3 Layers	4 Layers
Thickness [μ m]	0.8	1.2	1.6	2

Table 4.1: Multilayer thickness of Pt ink (Sint: 180°C@30min)

DS 10 μ m could not be measured due lines overlapping because substrate shows a low surface energy at low temperatures.

Also, a multilayer thickness profile was performed Figure 4.4. Obtaining table 4.1, it is observed that thickness is directly proportional to the number of layers.

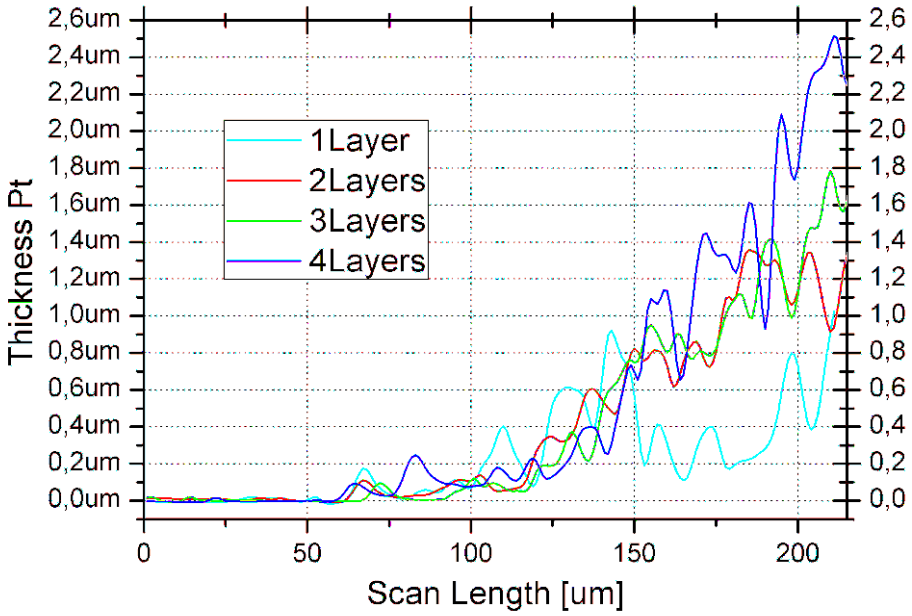

Figure 4.4: Printed arrays at different layers for Pt ink (DS25 at 25°C) (Sint: 180°C@30min). Curves show from substrate to inside of van der Pauw pattern

4.1.3 Sheet resistance

Electrical characterization of the printed patterns for different sintering conditions was done using various van der Pauw [28] patterns (Square 4mm x 4mm). Each van der Pauw pattern was sintered at different temperatures and times. Figure 4.5 a) shows the measured sheet resistance versus the sintering temperatures for the Pt ink used in this work. Starting at 180 °C Pt ink shown reasonable low resistance. As can be seen in Figure 4.5 a) that the best sintering condition is 200 °C. Finally, a sintering temperature of 180 °C for 30 minutes was selected for the conductive layers of the WE electrode, resulting a sheet resistance of about 6.3 $\pm$ 0.11 Ohms/square.

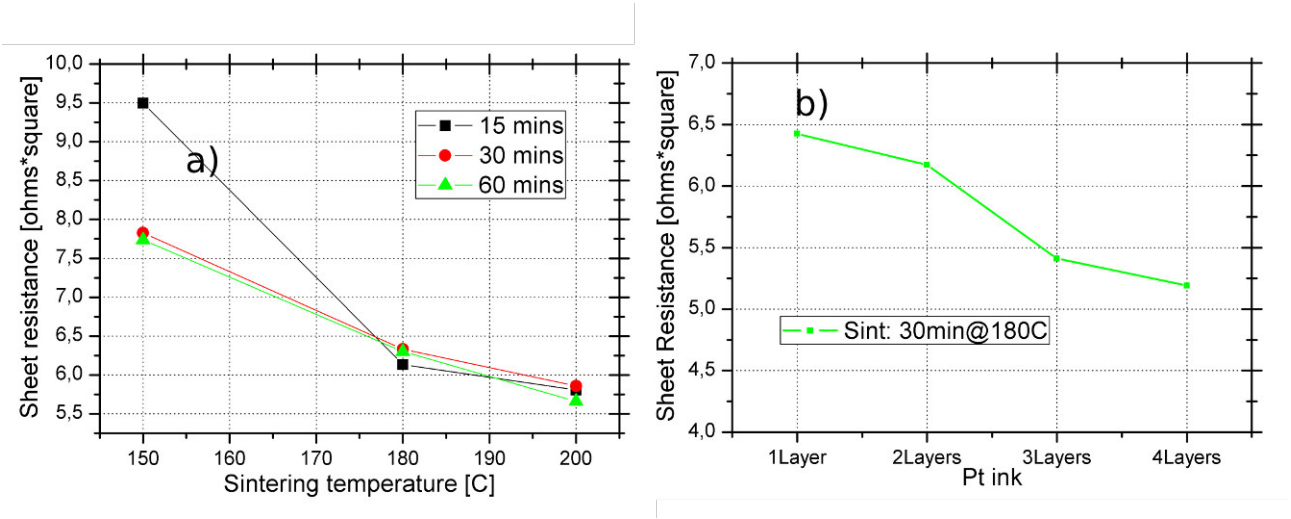

Figure 4.5: Sheet resistance measurement for a) different sintering temperatures and times Pt ink and b) Various Pt ink layers.

4.1.4 Pt Ink characterization

The morphology and topography of the printed layers with Pt ink were also studied. All these studies were done with Pt printed with DS25 at 180 °C

Morphological characterization by optical microscopy and SEM

The morphological characterization of the ink helps to understand its electrical behavior. Figure 4.6 shows an optical image of a Van der Pauw structure (Square 4x4 mm). In Figure 4.6 a) it can observed the quality of the printing, edges are pretty lined and also square has the designed size. However looking closer c) and d) the ink shows cracks.

Cracks can lead to a high resistance pattern. If cracks could be removed, ink could have less resistance. Nevertheless, as it has been detailed in the sheet resistance section, Pt ink exhibits low resistance.

Figure 4.7 shows SEM images of the inkjet-printed Pt ink before and after the sintering process on Kapton substrate. The removal of surfactants from the surface of the nanoparticles plays a significant role in enhancing conductivity of the printed films (Previous section). These images demonstrate that after the curing process, the particles are agglomerated, and a crack reduction is observed. Changes in particle morphology before and after the sintering process are hard to observe. the Pt particles, having a size of about 40 nm, neither melt nor deform at our working temperature of 180 °C.

In order to evaluate the sintering process and grain size development in a van der Pauw structure printed with DS25@180 a cross-sectional SEM was recorded after cutting the sintered Pt sample with a focused ion beam. Figure 4.7 b) shows the grain structure of the Pt Ink samples after the sintering at

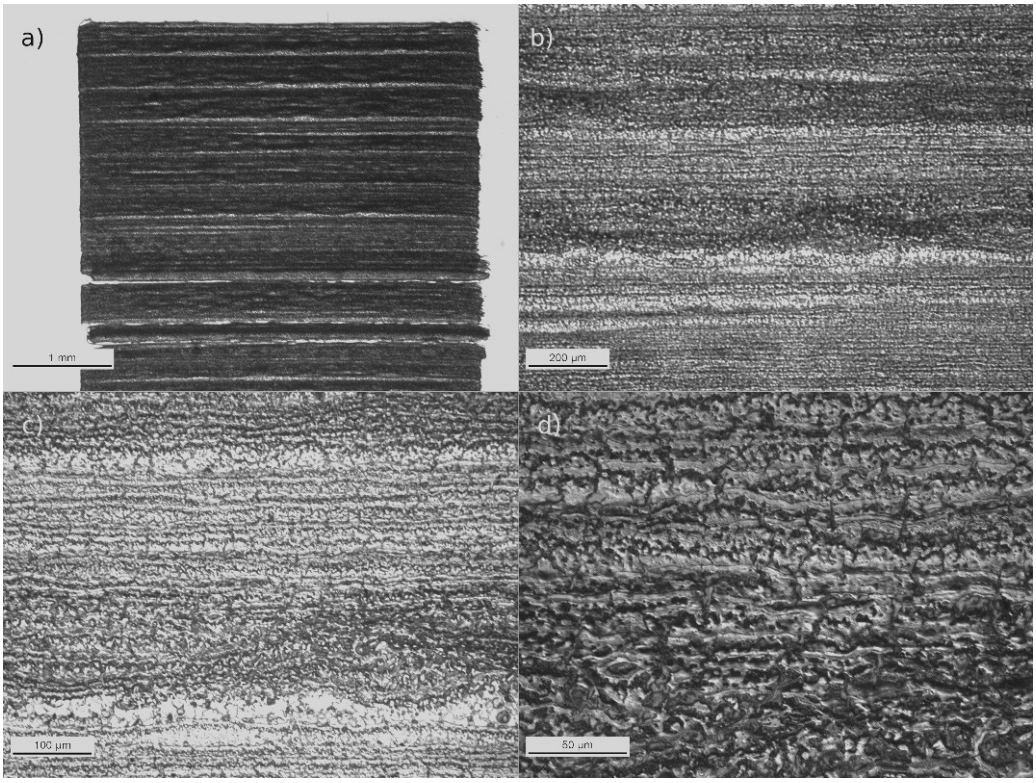

Figure 4.6: Morphology of the printed and sintered layers by Microscopy

180 ºC. It can be observed that the initial individual nanoparticles are transformed into larger clusters and hence a continuous network of Pt. The resulting grain structure and its density after the sintering, is the main parameter that affects on the final resistivity values. The final thickness of this structure is aproximately 350 nm.

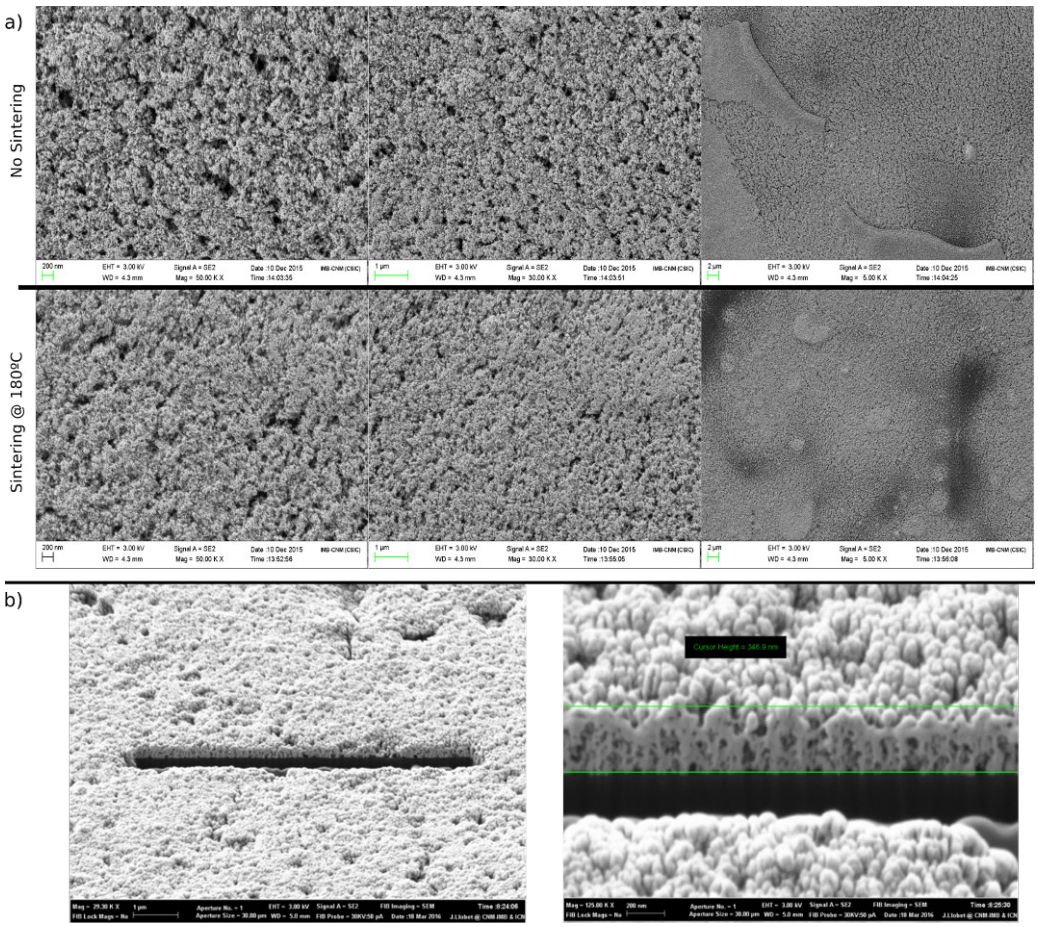

Figure 4.7: a)Morphology of the printed no sintered (upper row) and sintered (Lower Rows) layers by SEM, b) Cross-section SEM image of a single layer of sintered Pt ink

Topography AFM

Surface of Pt ink were also studied by AFM Figure 4.8. As can be observed the roughness of Pt ink is very high. The root-mean-square (RMS) roughness of the Pt electrode surface was about 118 nm.

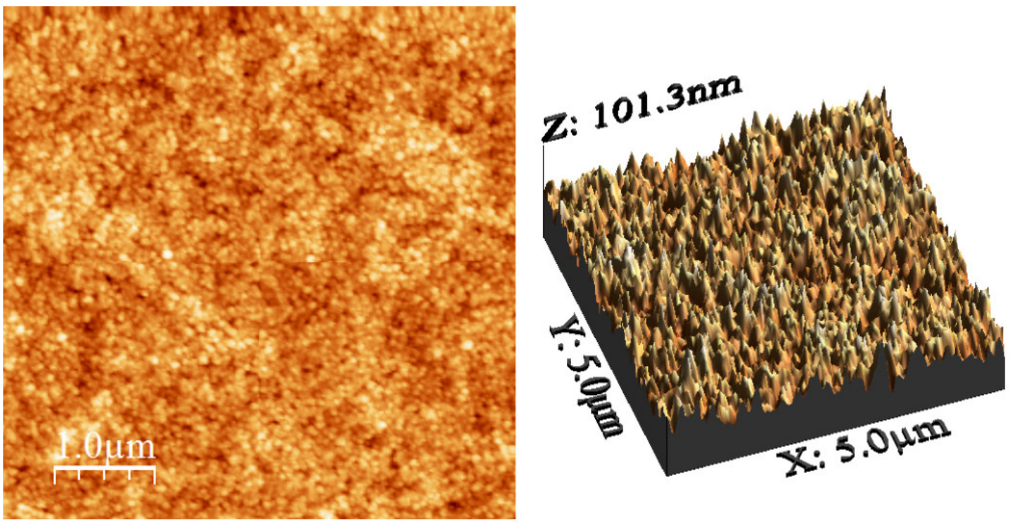

Figure 4.8: Morphology of the printed and sintered layers by AFM

4.2 SU8 ink print optimization as passivation

For the SU8 ink, the obtained single drop diameter was 46 $\pm$ 2 μ At a DS15, a line width of 69.0 $\pm$ 10 μ m was obtained. The thickness of the line for the selected DS is about 1.8 $\pm$ 0.05 μ (Figure 4.9 a) b). Thus, the SU8 layer is about nine times higher than the Pt layers due to the low amount of solvent in the ink formulation.

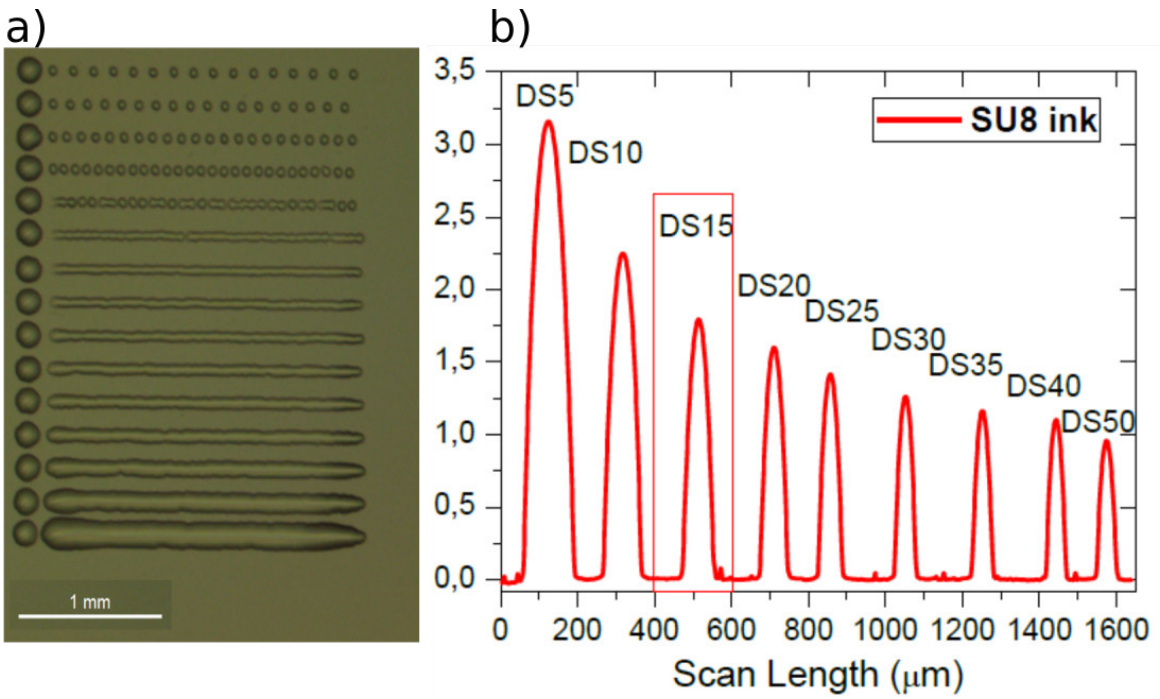

Figure 4.9: a) Printed lines at different drop spacing for SU8 ink images. b) Profilometer of line pattern

The passivation of the electrodes was done using the SU8 ink. SU8 was applied as the dielectric

material to print passivation patterns on the electrodes in order to precisely define the active area of the electrodes. As it is optically transparent this extended benefit in the future visual characterization of the printed structures.

4.3 Ag ink print optimization for pseudo-reference

In comparison with Pt ink, the single drop diameter of the silver ink was about 55 $\pm$ 1 μ m Figure 4.10) and the line width and line height at a DS of 40 μ m were determined to 53.1 $\pm$ 7.8 μ m and 233 $\pm$ 35 nm, respectively

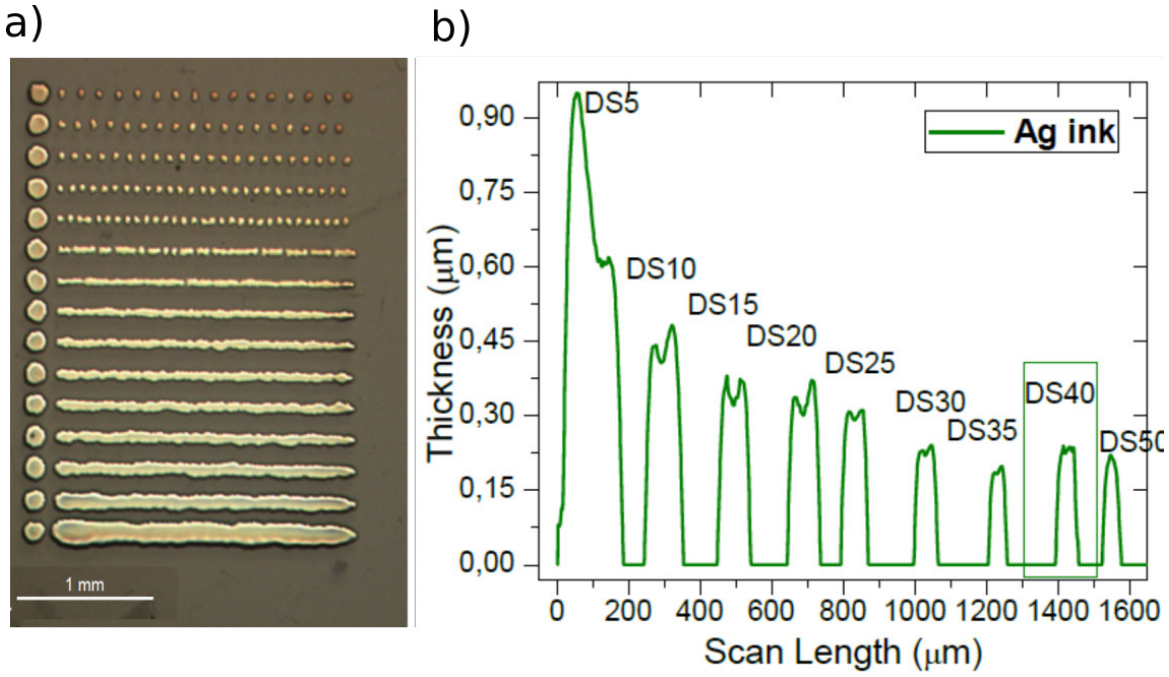

Figure 4.10: a) Printed lines at different drop spacing for Ag ink images. b) Profilometer of line pattern

As can be seen in Figure 4.11 For the silver ink, there are a clear agglomeration of the nanoparticles at 180 ^{o}C forming larger structures leading in less resistance. In addition, the root-mean-square (RMS) roughness of the silver layer about 14 nm.

Resistance of silver ink was checked in the probe table by Van der Pauw technique. Silver Ink prove a low resistance from 120 ^{o}C (0.36 ohms/square) in lower times. As far as can be seen in Figure 4.12 that the best sintering condition is 180 ^{o}C. As Pt ink is going to be sintered at 180 ^{o} C for 30 mins, at this sintering time and temperature, Ag exhibits a sheet resistance of 0.14 $\pm$ 0.2 Ohms/square.

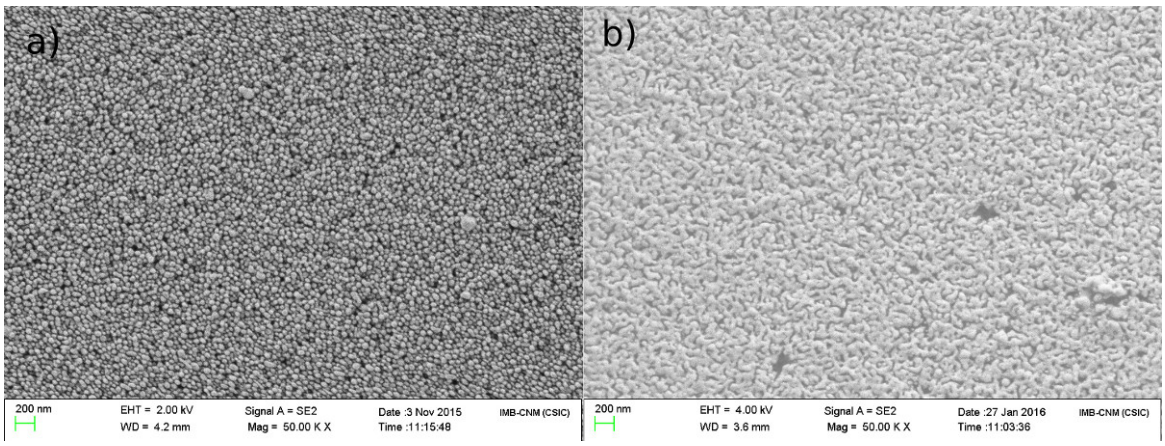

Figure 4.11: SEM images of Silver ink a) before and b) after sintering at 180 ºC

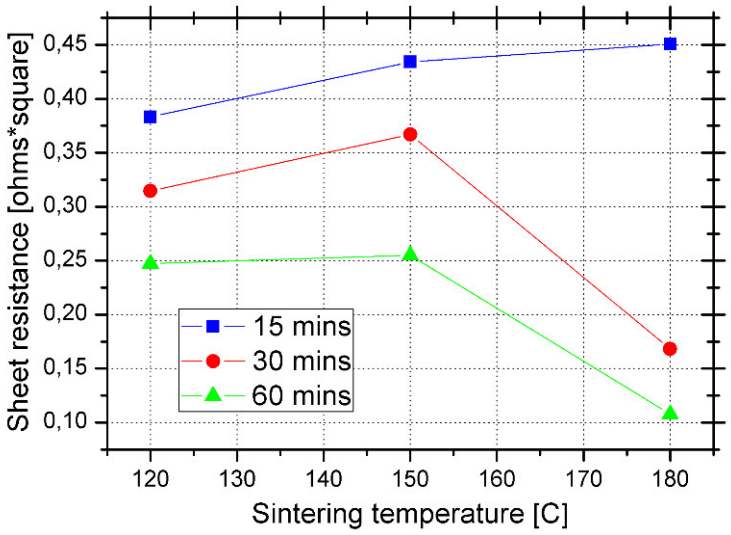

Figure 4.12: Sheet resistance measurement for different sintering temperatures and times Ag ink

4.4 Microelectrodes fabrication

The WE is printed on using a developed Pt nanoparticle-based ink, the pRE was produced by chlorination of silver nanoparticle-based patterns and the passivation was printed using SU8 ink.

This Master Thesis was performed using three different sizes of square WEs (Figure 4.14 b) for developing the pH sensor. The WEs was done of 1000 μ m x 1000 μ m (from now on, refereed as 1mm), 600 μ m x 600 μ m (from now on, refereed as 600 μ m) and 300 μ m x 300 μ m (from now on, refereed as 300 μ m). The use of square electrodes have been done because the previously standard fabricated platinum electrodes in the GAB group, used also this geometry (300 μ m [3]). The use of the same pattern enable a strict comparison of the microelectrodes, and so, their good performance.

The procedure for the manufacturing of the pH sensor is illustrated in Figure 4.13. The first step is the printing of the Pt nanoparticle ink for the development of the WE (Figure 4.13 a). The Pt ink was printed using a DS25. After the deposition process, the Pt ink cartridge was replaced by

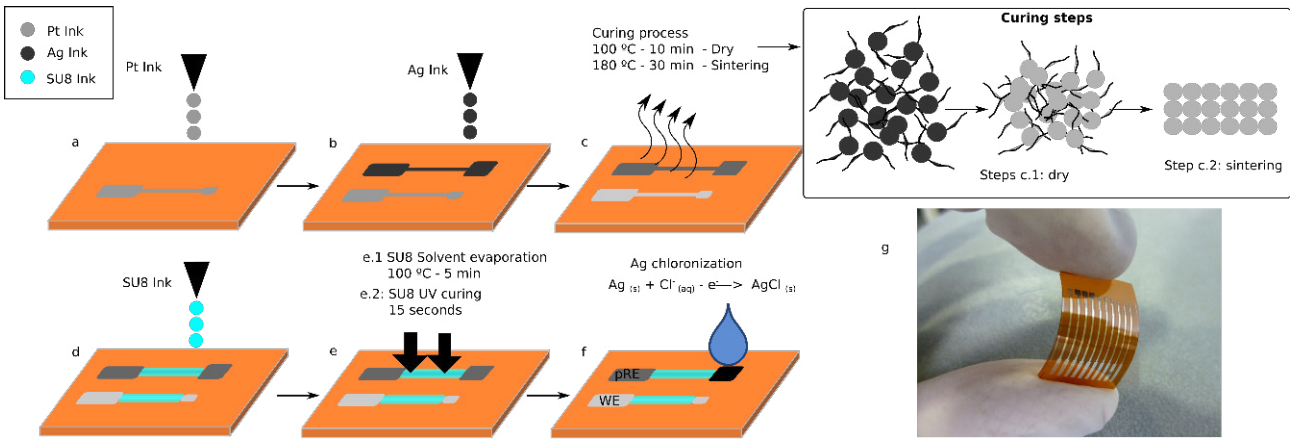

Figure 4.13: a) Inkjet printing of Pt WE, b) inkjet printing of silver pRE, c) thermal sintering of Pt and Ag layers, d) inkjet printing of passivation layer SU8, e) curing of SU8 at 100 ºC for 5 minutes and UV cross-linking for 15 seconds, f) Chlorination of the pRE, g) printed platform with 9 WE sensors and 1 pRE.

another cartridge containing the silver nanoparticle ink to print the pRE (Figure 4.13 b)). The DS for the printing of the silver ink was changed to 40 μ m Then, both printed inks were thermally dried and sintered. The temperature processing of the inks can be understood as two consecutive steps: First, drying for 10 minutes at 100 ºC of the layer is initiated expelling all solvent and decomposing polymeric stabilizing agents of the nanoparticles and second, a sintering process at 180 ºC for 30 minutes takes place fusing the nanoparticles. This ensured the electrical conductivity of the layer (Figure 4.13c.2). To precisely define the desired active electrode area and pad connections area, a passivation layer is formed by printing the dielectric SU8 (Figure 4.13 d). The SU8 ink has been already previously used as a passivation due to the high chemical resistance, the excellent thermal stability, the low Young's modulus, the low-temperature cure and is also optical transparency [47]. A cartridge was filled with SU8 polymeric ink to print on top of the Pt ink patterns aiming to precisely passivate the tracks. The DS used to print SU8 ink was 15μ m The curing of the SU8 was done in two steps, first heated at 100 ºC for 5 minutes for solvent evaporation and afterward by UV treatment for 15 seconds to polymerize the layer by cross-linking (Figure 4.13 e). After all the printing steps, the printed silver electrode was chlorinated to obtain a stable Ag/AgCl pseudo-reference electrode (pRE) [48] as shown in Figure 4.13 f. Figure 4.13g shows a picture of one complete platform with the two all-inkjet-printed microelectrodes (WE and pRE) that conform the final pH sensor. It can be observed that each fabricated platform includes three microelectrodes of three different dimensions (300 μ m, 600 μ m and 1 mm).

Figure 4.14 a) shows the pattern of this platform and Figure 4.14 b) a microscope image of the printed electrodes. The connection to the electrode pads was made by Zero Insertion Force (ZIF)

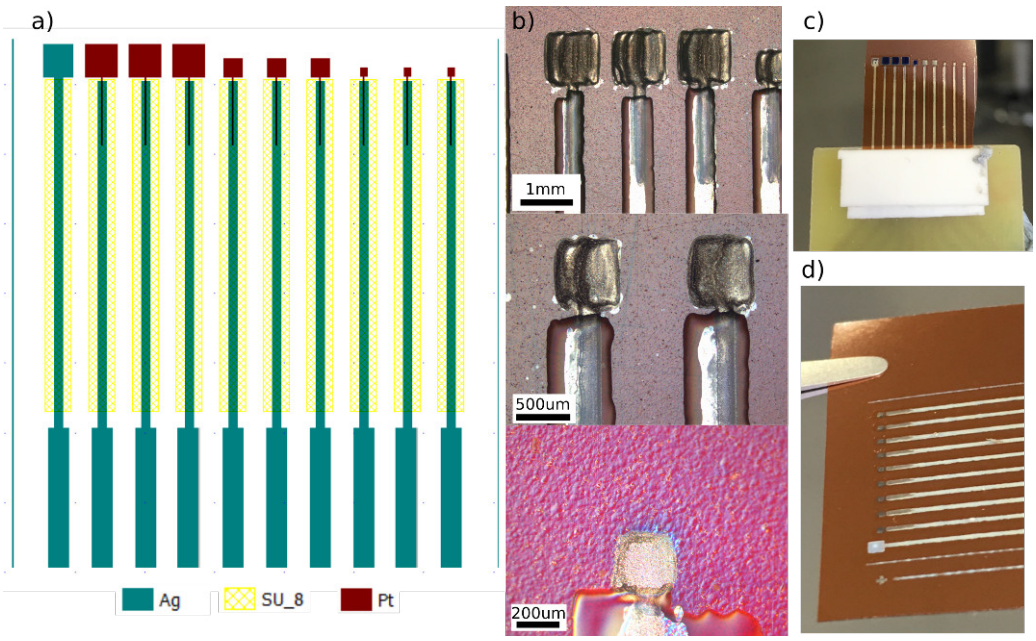

Figure 4.14: a) Pattern layout of the designed platform with three sizes of WE, b) microscopic image of the three WE made with inkjet printing, c) printed platform (3 sizes WE (300, 600 and 1mm)) with pRE connected, with a ZIF connector, d) printed platform of 9 WE of 300um with pRE.

connectors, thus avoiding other expensive methods such as wire-bonding. This strategy reduces the fabrication time, and it furthermore allows the reusability of the connectors. Figure 4.14 c) shows the fabricated platform connected with the ZIF connector. The connector can be reused for each platform and permits an easy connection to the multiplexor potentiostat of each configuration of electrodes on a different channel.

4.4.1 Passivation strategy

The passivation is the layer patterned over the metallic pattern in order to define the desired active electrode area. In this case, and as it will be detailed in the next sections, sometimes, it was observed some detachment of the Pt. So in order to avoid this problem, two different passivation strategies were used. The first one was the most easy, the passivation is only over the tracks, as can be seen in Figure 4.15 a). For the second one, it will be used the idea of ”donut”, just to describe that the passivation is also all around the electrode area, see Figure 4.15 b).

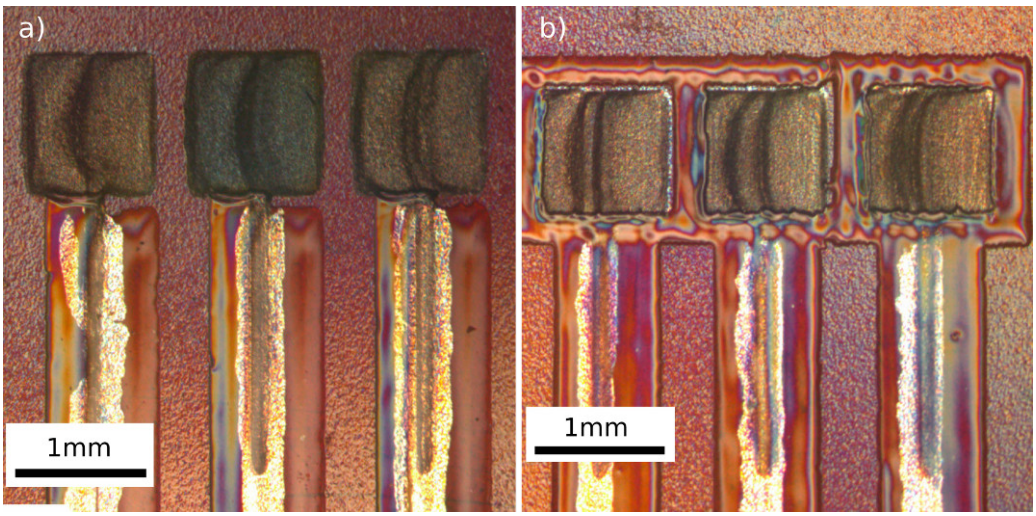

Figure 4.15: a) WEs passivated tracks and b) WEs with donuts passivation

4.4.2 Pseudo reference performance

Potentiometric measurements were performed in order to characterize the chlorinated Ag microelectrode to be used as reference element. The electrodes were immersed in 3M KCl and the potential stability was studied against a commercial Ag/AgCl RE for approximately 20h. In Figure 4.16 can be observed the potentiometric response of the sintered Ag ink, and the chlorinated Ag/AgCl ink. As can be observed, to stabilize the response a preliminary conditioning step is necessary. For Ag ink, after an initial marked drift, it can seen that the signal changes a lot and no stabilization is achieved. This is the main reason why the Ag ink is chloronized. For the Ag/AgCl electrode after the first 2 hours of conditioning step, the signal stabilizes and the noise is significantly reduced. It can be calculated the sensor drift for each material, obtaining an Ag drift of 1.6 mV/h and a Ag/AgCl 0.4 mV/h. For a robust RE the drift must be minimum in order to do not alter the final measurements, however, when using pRE electrodes this effect must be taking into account. The drift basically affects when the experiment is long in terms of time.

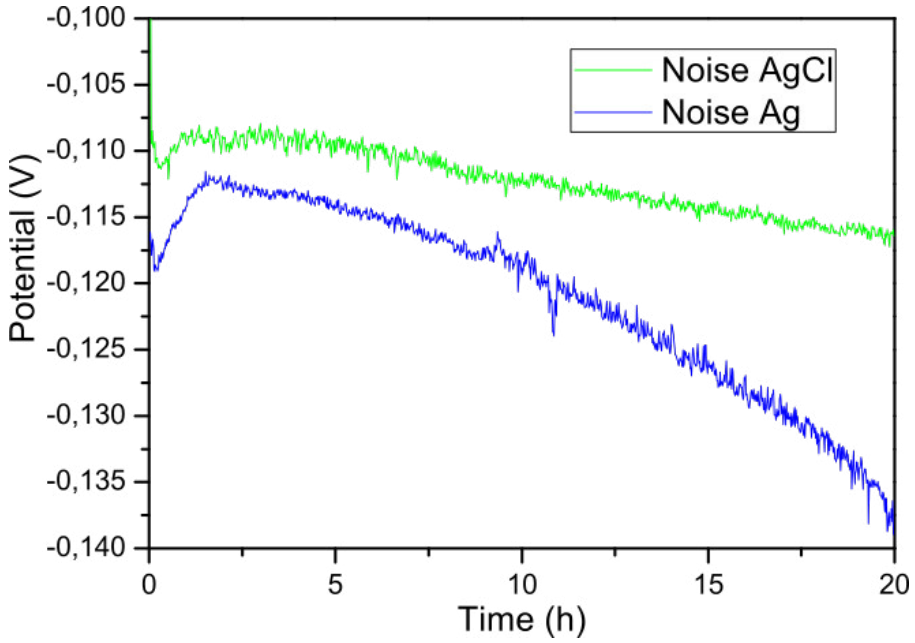

Figure 4.16: Potential stability of the developed pRE over time

4.5 Electrochemical characterization of Pt microelectrodes

As it has been explained before, the work will begin using platinum microelectrodes, and then this surface will be modified with an electrodeposited iridium oxide. In order to determine the change of properties through the coating, it is necessary to characterize the bare electrode first. This characterization will be done basically with impedance and cyclic voltammetry both for Pt and AEIROF microelectrodes.

4.5.1 Impedance measurement

In order to determine the change of properties, it is necessary to characterize the bare electrode first. In the following Figure 4.17 it can be seen the results of an impedance measurement. The parameters for characterization were taken from [49].

Depending on the application, sometimes it is required the use of small area electrodes. The measured impedance response for the three different studied electrode dimensions is shown in Figure 4.17. The Bode plot is segmented in two parts (Magnitude and Phase) to provide more clarity in observing the impedance response. In the low frequency region, the effective surface area is a significant feature. The impedance decreases with an increasing of active surface area of the electrode in the electrolyte. Because large surface area allows more charge to pass by and thus reduces impedance. Not only have the dimensions, also the roughness of the material, changes the active area of the electrodes. As it was presented in section 4.1.4, the printed Pt electrodes showed a high roughness. This roughness implies

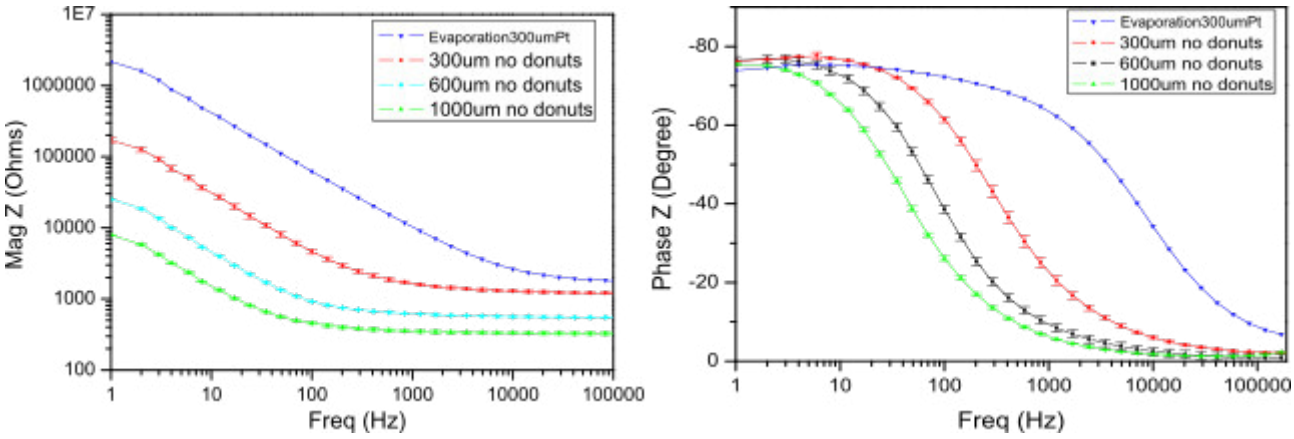

Figure 4.17: Bode-plot of electrodes (n=30)

the reduction of the impedance. This effect was studied comparing the impedance of a Pt printed electrode against a another Pt electrode fabricated by evaporation (Bilayer Ti/Pt 30+180 nm) with standard microelectronic techniques both with the same dimensions (300 x 300 μm). Evaporation achieves more homogeneous and planar electrodes compared with printed technique (RMS=6 $\pm$ 1 nm [50]). In Figure 4.17 can be observed the impedance of electrodes. As it was expected, printed Pt electrodes had higher active area achieving small impedance values. This is a big advantage due to the electronic equipment for the measurement of impedance can not work with high impedance values. When is necessary to reduce the impedance, but maintaining reduce area of electrode, one of the used strategies is to deposited roughness materials (as black Pt) onto the surface to increase the active area of the electrodes [54]. With printed Pt electrodes is is not necessary to make this deposition since small area can be measured without problem thanks to the roughness of the material.

Also, electrodes with donuts passivation were measured (Figure 4.18). As can analyze of Figures 4.17) and 4.18), the major difference is a major dispersion in electrodes with donuts, a reason why for this Master Thesis the main work was performed with electrodes without donuts.

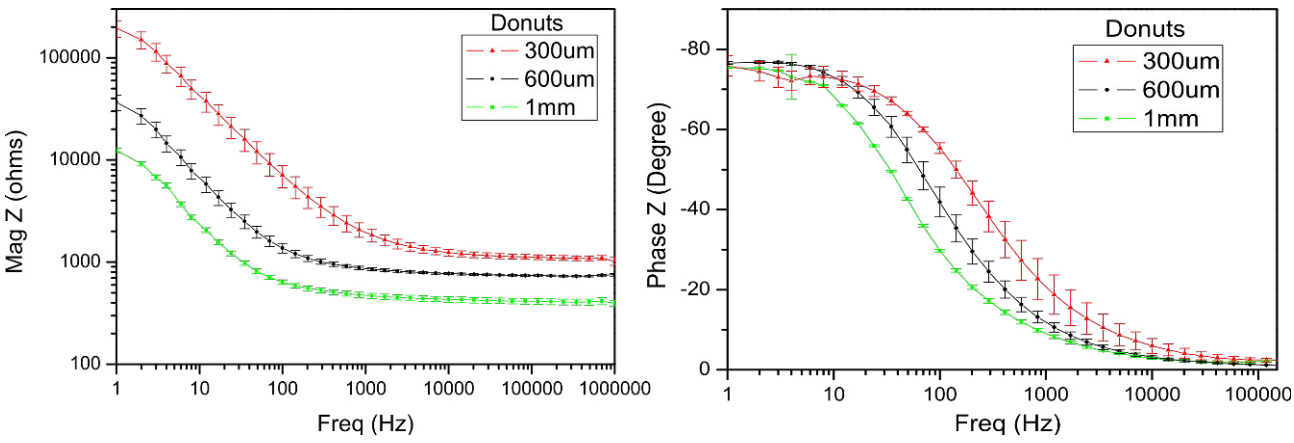

Figure 4.18: Bode-plot of electrodes with donuts passivation (n=30)

Impedance measurements are made using an AC signal, where the current oscillates in a sinusoidal manner from as low as a few hundred to nearly 1,000,000 Hz in different measurements. Using AC instead of DC signals to monitor the cells upon electrodes has two important consequences.

First, an AC source is used to prepare solution avoiding electrolyte till electrode is place, causing the properties of the electrodes to change or polarize. The use of an AC signal also offers another very significant advantage, An AC analyzis is capable of monitoring both the voltage and the phase of the voltage relative to the current. Combining these parameters, the impedance can be broken down into two parts: one due to pure resistance and the other to the reactance of the system. The reactive part (Xc) in this case is due to the capacitance (C) associated with the metal surfaces in the solution (the electrolyte). It can now report changes over time in the pure resistive (R) as well as the capacitive portions (C) of the impedance. Knowing R and C it can be obtained a equivalent circuit. Figure 4.19 shows several equivalent circuits that can be used to understand the electrode-electrolyte interface.

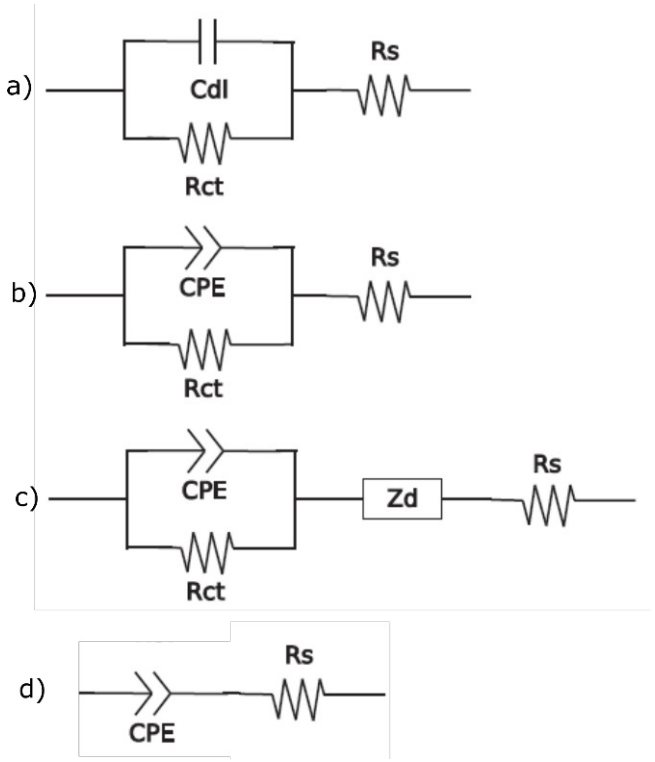

Figure 4.19: Equivalent circuits used to fitting the electrodes characterization data.

The equivalent circuit models can be divided into two parts, one related to the access resistance and the other to charge transfer at the electrode double layer. The components used to describe each phenomenon depend on the electrode materials properties. The access resistance is modeled by the solution resistance Rs. Rs mainly depends on the geometric area of the electrode and the conductivity of the solution. the electrode double layer behaves as a capacitance. However, to achieve a better representation of the dissipative double layer behavior it is necessary to substitute the pure capacitance

	CPE_T	CPE_P	R_s
1 mm	$1.99x10^{-5} \pm 6x10^{-7}$	0.856 ± 0.007	334.9 ± 3.5
600 μ m	$5.9x10^{-6} \pm 1x10^{-7}$	0.868 ± 0.005	574 ± 4.8
300 μ m	$9.2x10^{-7} \pm 2.x10^{-8}$	0.854 ± 0.004	1250 ± 12.4

Table 4.2: CPE and Rs values for WE dimensions

by a faradaic pseudo capacitance known as the constant phase element (CPE).

Analyzing the behavior of electrodes in magnitude and phase in Figure 4.17, it represents a behavior of a CPE and a resistance, therefore the equivalent circuits that best fit in the behavior of electrodes corresponds to the circuit d) in Figure 4.19. The impedance of this equivalent circuit is defined in 4.1:

$$Z = Z_{CPE} + R_s = \frac{1}{CPE_T(j\omega)^{CPE_P}} \tag{4.1}$$

In table 4.2 CPE and Rs values are shown, These values are obtained by applying equation 4.1 in Z results (4.17). CPE and Rs values are a useful tool to establish electrical comparisons between electrodes.

4.5.2 Cyclic voltammetry

The cyclic voltammetry in PBS to determine the charge storage capacity of the manufactured electrode was performed (Figure 4.20). Depending on the ability of the electrode to store charge, a more or less pronounced hysteresis can be observed. In Figure 4.20 stored electrodes charges are proportional to WE active area. Therefore, it is estimated that the stored charge per unit is equal in the three WEs dimensions.

In the same way, the behavior of the different dimensions of WEs were tested. Figure 4.21 shows the CV in ferro(II)/ferri(III)-cyanide obtained for three different dimensions of WE. The anodic/cathodic peak current values (Ip) are directly proportional to the WE area as shown in the theoretically Randles-Sevcik equation (Figure 4.21 b). The Ip shows when all of the atoms in the vicinity of the working electrode has already been reduced or oxidate. To determine if the electrodes are working properly we compared the obtained Ip with the theory (Table 4.3), using Randles Sevcik's equation [51]. As can be seen in Table 4.3 Ip values are consistent with the theoretical values of Randles Sevcik, in this manner the proper function of the electrodes are shown.

Moreover, the printed electrodes have heterogeneous behavior onto the plastic substrate causing different electrochemical properties of the electrodes. Another parameter of interest for the characterization of the electrodes is the peak-to-peak separation ($\triangle E$) over a range of Scan Rate. $\triangle E$ is

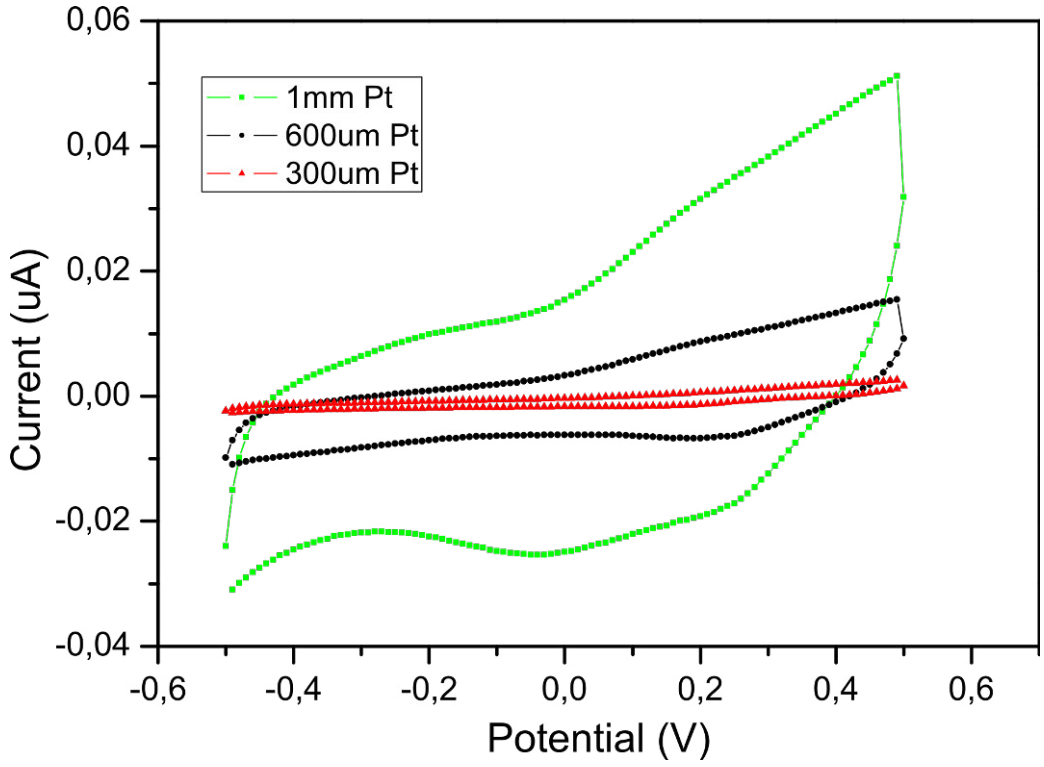

Figure 4.20: Cyclic voltammetry in PBS for the three WEs.

		Theorical	Experimental	Experimental	Theorical
WE	Real Areas [mm^2]	Ip [μA]	Ip [μA]	$\triangle E$ [mV]	$\triangle E$ [mV]
1mm m	1.06	$1.87x10^{-5}$	$1.67x10^{-5}$	60	59
600 μ m	0.317	$6.16x10^{-6}$	$6.16x10^{-6}$	60	59
300 μ m	0.073	$7.33x10^{-6}$	$1.13x10^{-6}$	60	59

Table 4.3: Ip and $\triangle E$ of three electrodes dimension at 20mV/s vs Theoretical values from Randle Sevciks equation

the potential difference between anodic Ip and cathodic Ip. The reduction of ferri(III) to ferro(II) cyanide is a one electron process for which, under fast electrode kinetics, a $\triangle E$ of 59 mV at room temperature is anticipated [52]. Our printed electrodes display a $\triangle E$ around 60 mV at low scan rates (Table 4.3). Ip and $\triangle E$ theorical values demonstrate that the Pt electrodes are functional and have a good electrochemical response.

Our printed electrodes display a $\triangle E$ around 70 mV until scan rate of 100 mV/s. There are a number of possible reasons that may increase the $\triangle E$ larger than the theoretical 59 mV, most probably small holes, cracks, wettability of the electrodes and organic contamination still remaining after the drying and sintering process [53]. At faster scan rates (Figure 4.22) an increment in $\triangle E$ experimental results is shown straying from the theoretical values. This is due to quasi-reversible

	Ip	Ip	$\triangle E$	$\triangle E$
Scan Rate	Theorical	Experi	Experi	Theorical
mV/s	A	A	mV	mV
5	3,96E-06	3,81E-06	70	59
10	5,5941E-06	5,53E-06	60	59
25	8,84504E-06	9,73E-06	60	59
50	1,25088E-05	1,44E-05	70	59
75	1,53201E-05	1,77E-05	70	59
100	1,76901E-05	1,98E-05	70	59
200	2,50176E-05	2,90E-05	90	59
500	3,95562E-05	4,64E-05	130	59
1000	5,5941E-05	6,64E-05	150	59

Table 4.4: Ip and $\triangle E$ at different scan rates using Randle Sevciks equation for a 600 μ m WE

kinetics of the electron transfer at the printed electrode. The value of the electron transfer rate constant was calculated using the approach described by Matsuda and Ayabe [55]. Table 4.4 and Figure 4.23 shows for the 600 μ m WE that the peak current increases linearly as a function of the square root of the scan rate (until 100 mV/s) as is typical for a diffusion-controlled process. This is represented in Figure 4.22 where it can be seen that at low scan rates the electrodes behaves ideally, and for faster scan rates has deviation from theoretical values. This will be object of study in the nearly future.

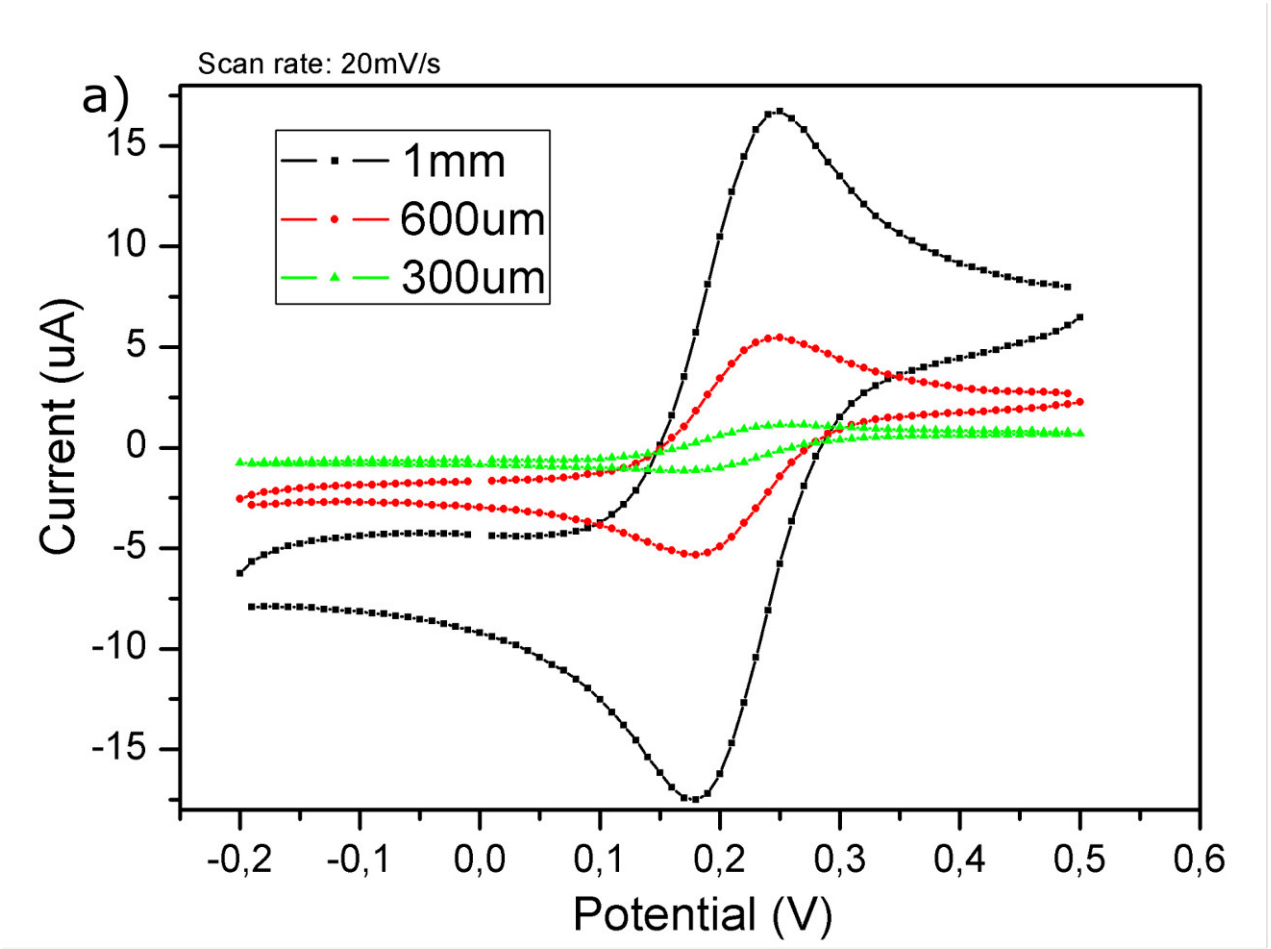

b)

$$i_p = 0.4463\, nFAC\left(\frac{nFvD}{RT}\right)^{\frac{1}{2}}$$

- C = concentration in mol/cm^3
- v = scan rate in V/s
- R = Gas constant in VC K^{-1} mol^{-1}
- T = temperature in K
- i_p = current maximum in amps
- n = number of electrons transferred in the redox event (usually 1)
- A = electrode area in cm^2
- F = Faraday Constant in C mol^{-1}
- D = diffusion coefficient in cm^2/s

Figure 4.21: a) Cyclic voltammetry of $K_3Fe(CN)_6/K_4Fe(CN)_6$ redox couple in 0.1 M KNO_3, varying electrodes sizes. b) Randle Sevcik equation

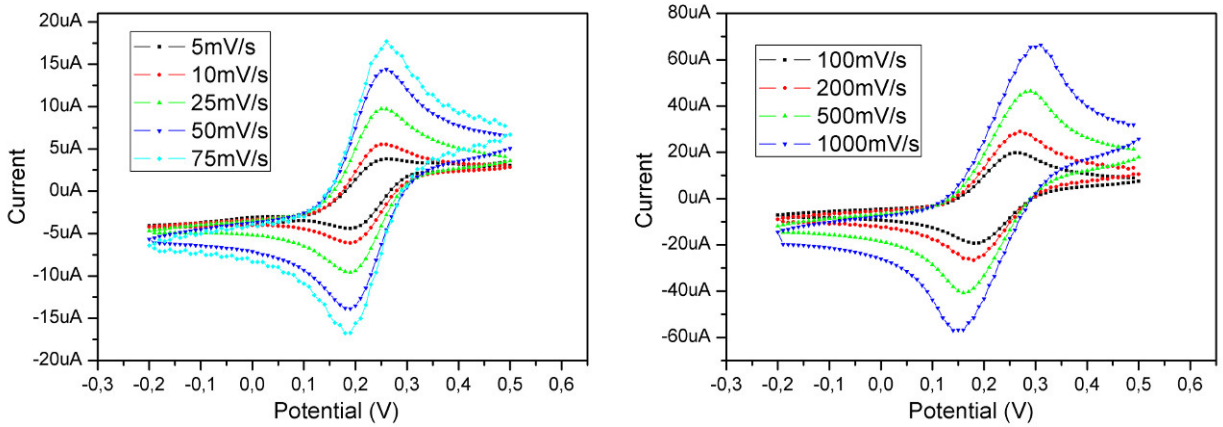

Figure 4.22: Cyclic voltammetry of $K_3Fe(CN)_6/K_4Fe(CN)_6$ redox couple in 0.1 M KNO_3, varying scan rate from 5 mV/s to 1000 mV/s in a WE of 600 μm.

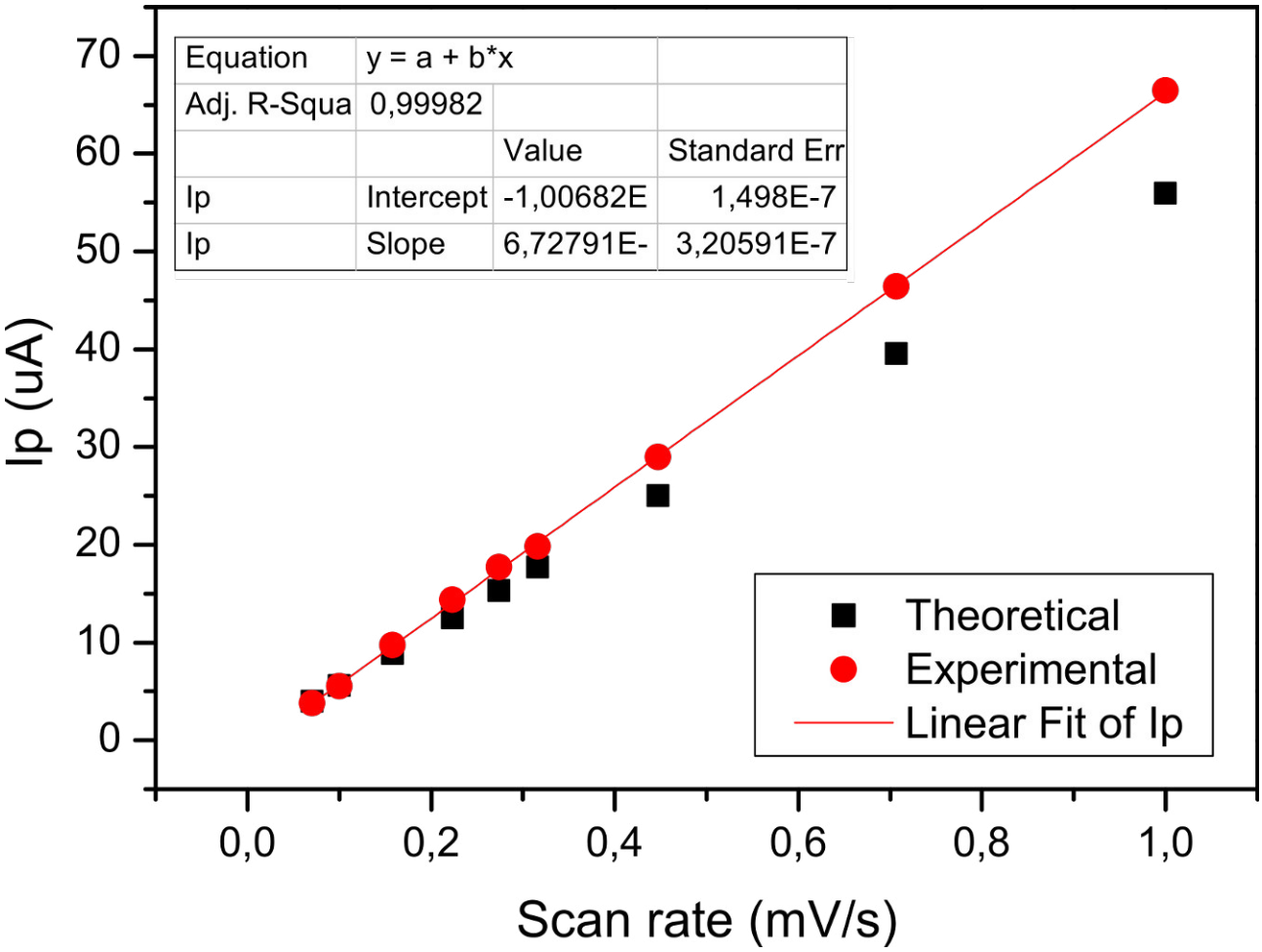

Figure 4.23: correlation of the theoretical versus experimental Ip in function of square root of the scan rate using the Standard Randles Sevcik equation for a 600 μ m WE

4.5.3 Electrochemical Activation

In electrochemical experiments, the quality of the active surface will affect the measurements. The peak currents in cyclic voltammetry and the frequency response during electrochemical impedance measurement will be dependent on the surface composition of electrodes. Upon exposure to a non-cleanroom laboratory environment the electrode surface is subject to numerous ambient contaminants, affecting binding kinetics of thiols in addition to electrochemical effects [30].

It is reported in literature that electrochemical activation is very important to ensure a good performance of the electrodes [29]. In these literatures, electrodes after activation show a larger charge storage capacity and the Ip and $\triangle E$ experimental values get close to theoretical ones. As can be seen in Table 4.3 the experimental Ip values are a little bit lower than the theoretical ones. So, electrochemical activation was applied to electrodes as in previous works, in order to improve electrodes electrochemical behavior.

Electrochemical activation was performed in the three WEs applying five pulses alternating between -2V and 0 V for 10 seconds in electrolyte solution. The idea of this activation is to generate H_2 gas at the surface of the electrode at negative potential. In Figure 4.24) charge storage capacity of WEs before and after activation is represented. The charge storage capacity does not show an important change before and after activation in any of WEs, therefore electrochemical activation does not modify charge storage capacity of Pt electrodes.

Also in Figure 4.25 the cyclic voltammetry in Ferro/Ferri cyanide of WEs before and after activation is represented. the Ip and $\triangle E$ does not show an important change before and after activation in any of WEs, therefore electrochemical activation is not useful to get accurates Ip and $\triangle E$ experimental values.

Moreover, once activation is carried out, WEs lose adherence to the substrate as it is shown in Figure 4.26. adhesion lost can be explained due a excessive current during the activation process.

Thus, after the presented activation results, it can be conclude that electrochemical activation does not show a significant improvement in electrochemical response. Morevoer, it must be taken into account the lack of adherence when the activation is done. All this makes that for the preparation of the Pt microelectrodes the activation will not be done.

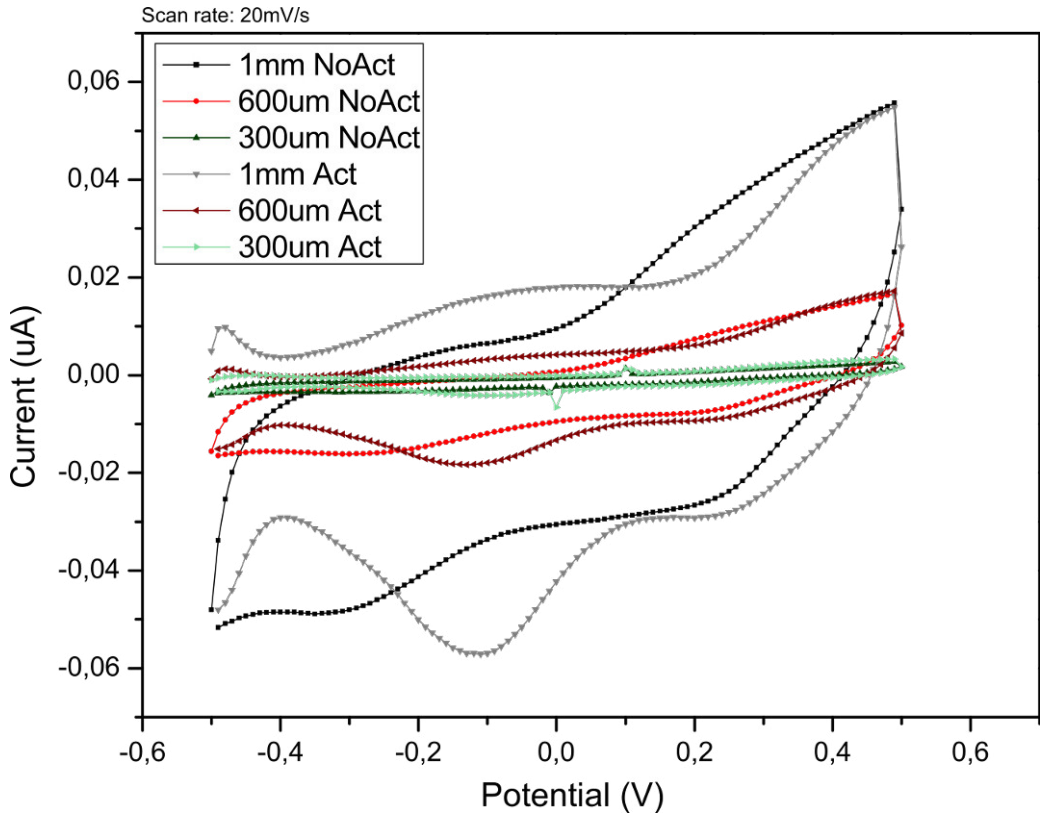

Figure 4.24: Cyclic voltammetry in PBS 20for the three WEs before and after activation at 20 mV/s.

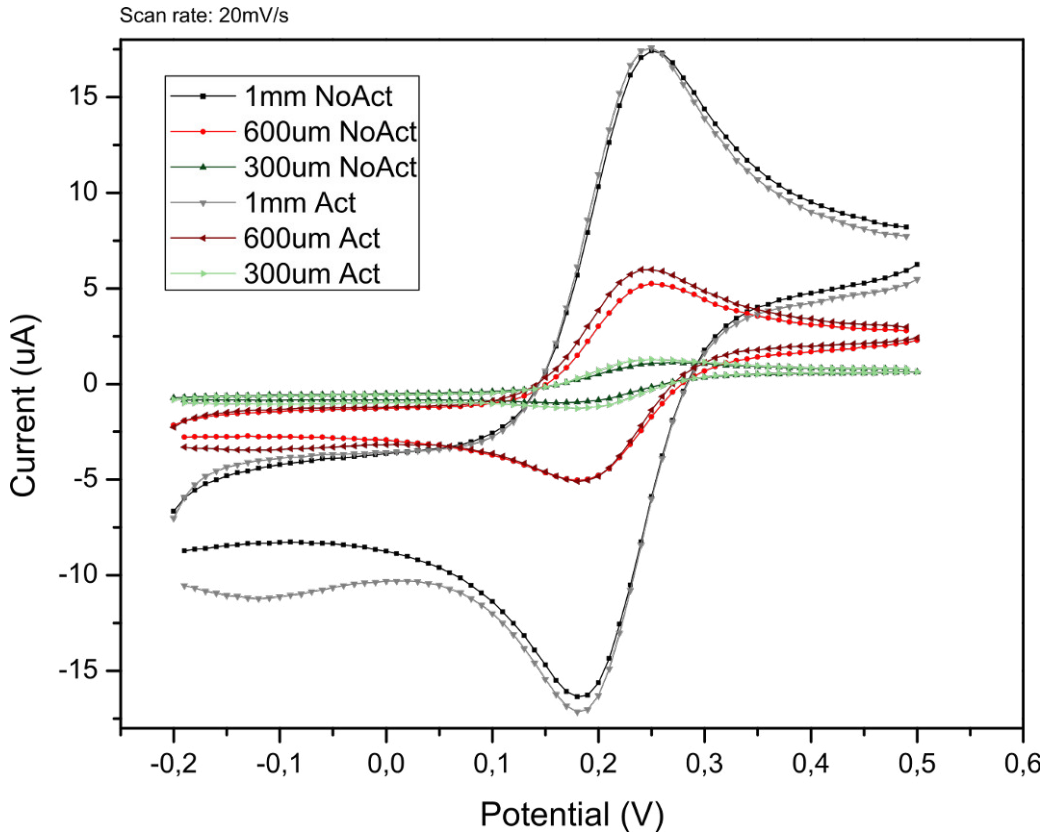

Figure 4.25: Cyclic voltammetry of $K_3Fe(CN)_6/K_4Fe(CN)_6$ redox couple in 0.1 M KNO_3 for the three WEs before and after activation at 20 mV/s.

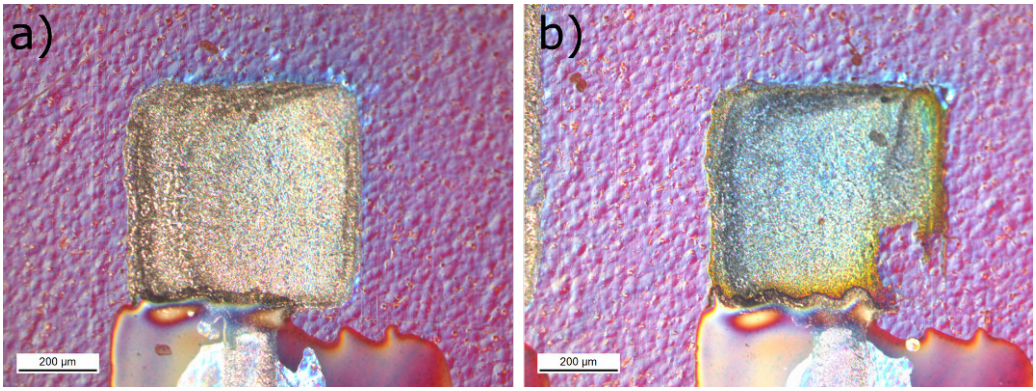

Figure 4.26: Images of electrode a) before activation and b) after activation

4.6 Electrochemical characterization of AEIROF microelectrodes

The platinum electrodes were coated with AEIROF via dynamic voltage sweeps as well. Under the microscope a change of color from Pt to blue could be observed due to this coating. During long-term observations, the stability of the resulting coatings has to be ensured. The amount of material on top of the electrode is responsible for the color (Figure 4.27). Different AEIROF growth conditions where tried (basically varying the number of sweeps) and the most optimum one achieved was 50. The impedance Bode Plot (Figure 4.28) and CVs (Figure 4.29) for each electrode was done. As expected, the presence of iridium oxide material changes the electrochemical behaviour in the following way: increases the charge storage capacitance and decreases the impedance at lower frequencies. This denotes that the AEIROF is a higher roughness material rather than Pt.

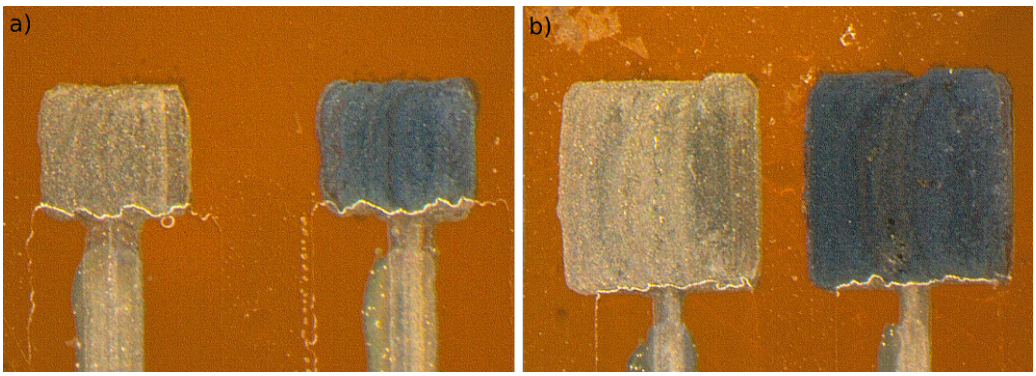

Figure 4.27: Microscopy images Pt (Pt color) vs AEIROF (blue) deposited a) WE of 300 μ m y b) WE of 600 μ m color differences at the same voltage sweep

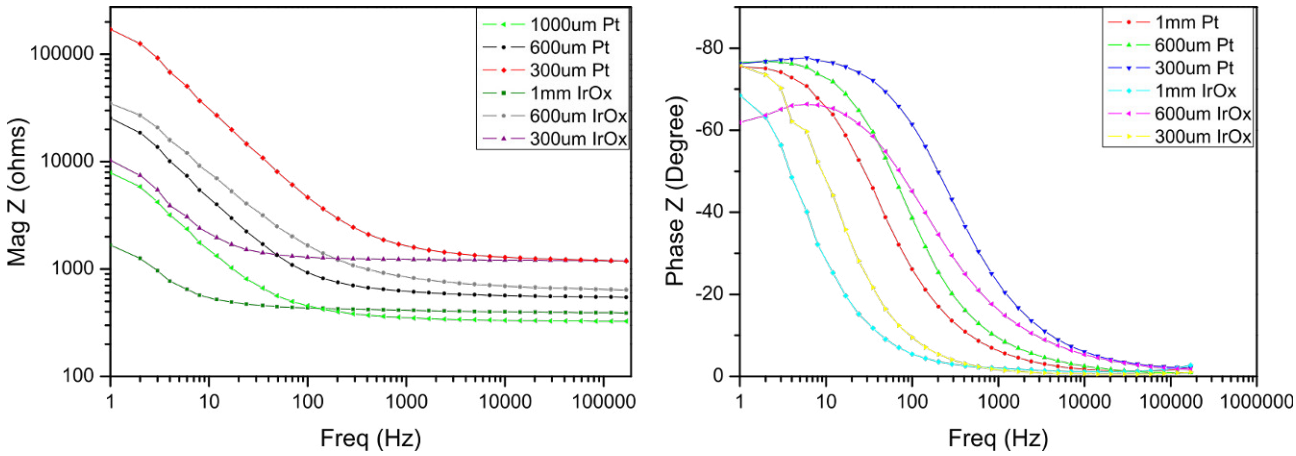

Figure 4.28: Impedance Bode-plot of bare Pt electrodes vs AEIROF for the three different dimensions.

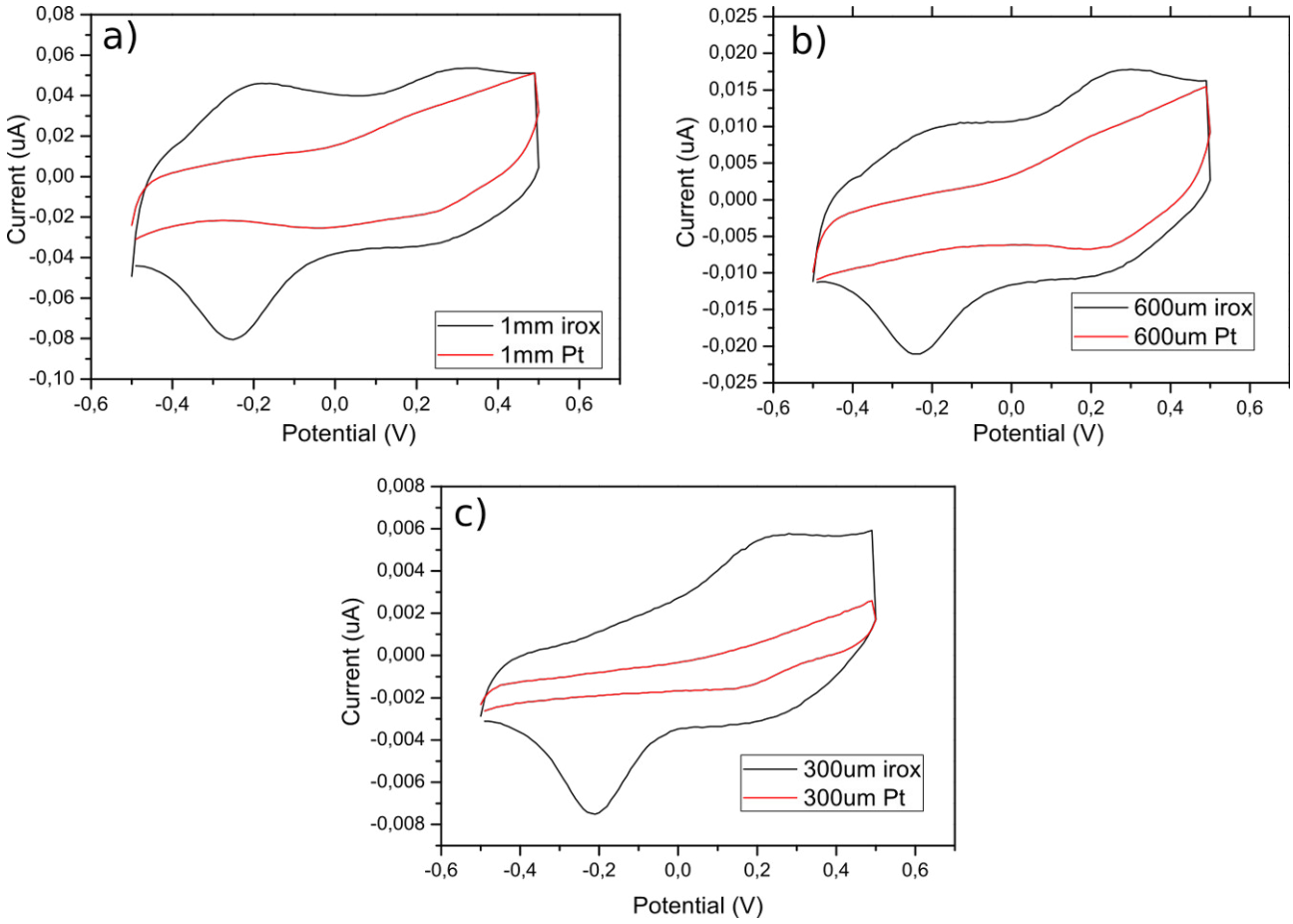

Figure 4.29: Cyclic voltammetry in PBS at 20 mV/s, comparison between Pt and AEIROF electrodes a) 1mm WE, b) 600μm WE and c) 300 μm

4.7 pH sensor calibration

The implementation of iridium oxide films (IROF) electrodes as pH sensors has been widely described as has been described in the introduction. One of the most accepted theories that can explain its working principle is that IROF intercalates protons within its structure when pH changes. This electrode modification can be measured by registering the electrode open circuit potential, which can be directly correlated with solution pH. Specifically in this work, potentiometric pH measurements were initially carried out by registering open circuit potential of an AEIROF-coated electrode against an external Ag/AgCl reference electrode. Figure 4.30 shows the response of an AEIROF pH sensor of 600 μ m in a pH range between 1 and 11. To ensure pH steps the measure was paused to change pH solution with the help of a commercial pH meter.

As expected, no significant differences in potential pH response, measured in terms of slope value, were observed between sensors dimensions. Showing that active area of WE does not influence in sensor performance. As it has been previously described in the literature, the AEIROF pH sensor exhibited a linear super-Nerstian response between pH 1 and 10, with averaged slope of 0.065 V/pH

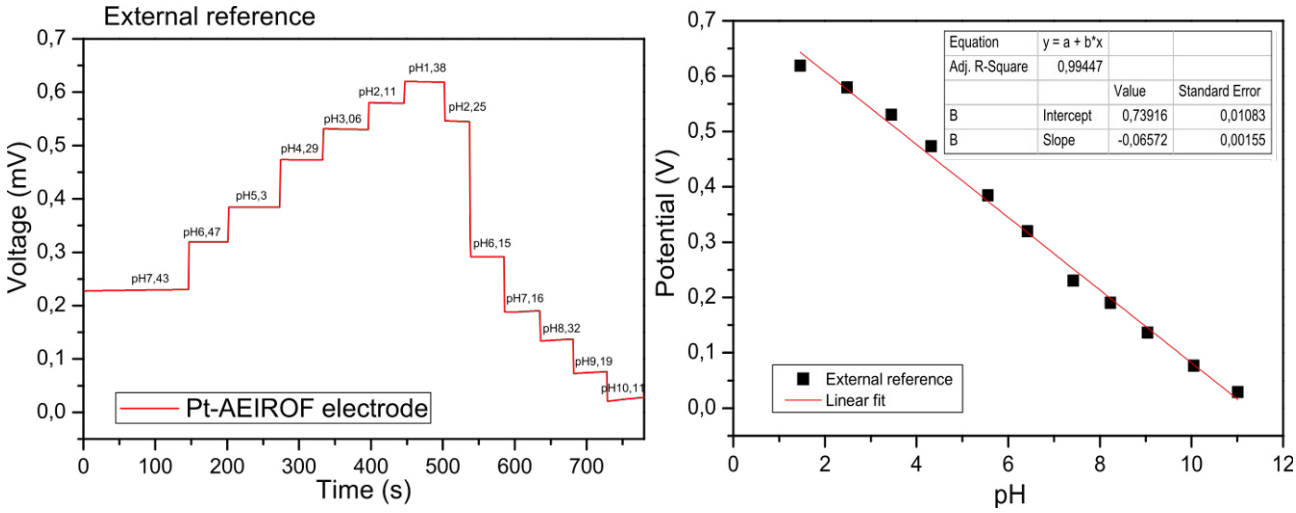

Figure 4.30: a) Response of the AEIROF pH sensor. b) Linear regression obtained for AEIROF electrodes.

and response speed of less than a second.

pH platform calibration with an integrated Ag pseudo-reference

Finally, we assayed pH monitoring using the internal pRE, which should facilitate handling sensors and detection in small sample volumes. The calibration plots recorded in Figure 4.31 against a commercial Ag/AgCl reference electrode and the internal pseudo-reference were comparable and showed similar response times, linear pH range and slope.

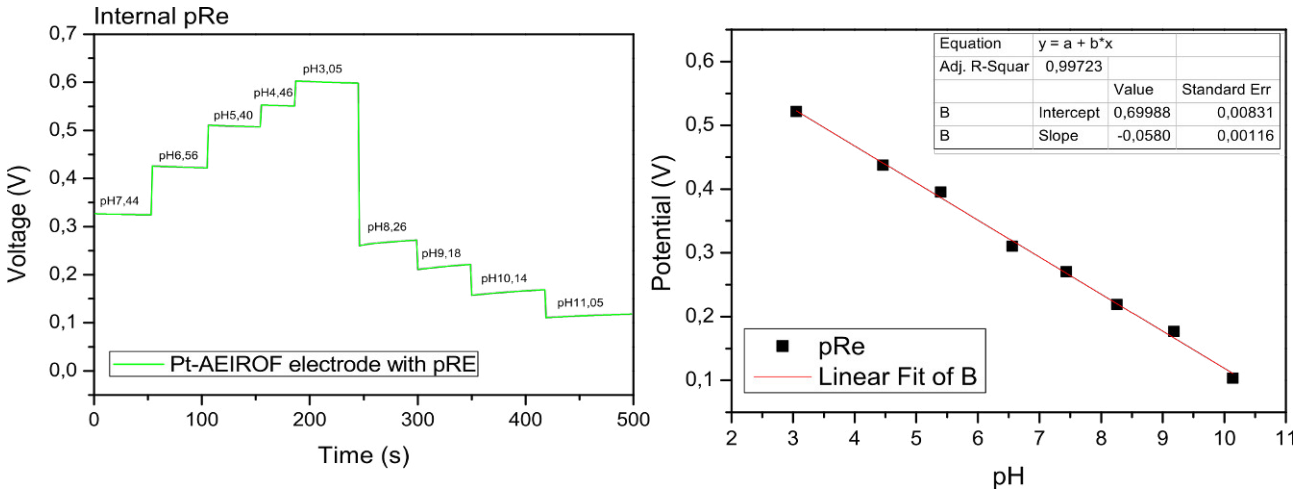

Figure 4.31: a) Response of the AEIROF pH sensor with pRE. b) Linear regression obtained for AEIROF electrodes.

Measurement of Figure 4.31 must have a drift of 0.08mV according to the calculated stability of pRE above.

Chapter 5

Conclusions

With the passage of the time, the electrochemical devices are becoming more and more sophisticated and versatile with dramatically shrinking in size and cost. Inkjet printing methodology offers the advantage of production of simple, economical, disposable, portable and mass produced devices suitable for a wide range of applications.

In this work is demonstrated the manufacturing of a pH sensor based on inkjet printing. The manufacturing strategy presented for the development of a pH sensor is very attractive due to its simplicity and rapidity. The sensor consists in two electrodes that were patterned on a flexible polymer substrate: Pt for the development of the WE and Ag for the pRE. Moreover, SU8 ink was used as a dielectric material to passive the tracks and define the active area of the electrodes.

The selected conductive nanoparticles inks used in this work were completely characterized in terms of printability and electrical and morphology properties. Both inks showed low-curing temperatures with good conductivities already from 180ºC for the Pt ink and from 120ºC for the Ag ink. The careful selection of low-curing ink formulations and the optimization of the inkjet printing as well the drying and sintering process allowed the manufacturing of the sensor at low temperature and in short time allowing its manufacturing in low-cost plastic and flexible substrates. The dielectric SU8 was cured by UV for 15 seconds.

This work provides an exhausted characterization of the printed electrodes. Different dimensions of square WE (300, 600 and 1000 μm) were studied. All the tested platforms exhibit the expected response in terms of electrochemical response. The obtained values were comparable with theoretical Randles-Sevick calculated ones. Moreover, printed Pt electrodes showed low impedance values due to the high roughness of the printed material compared with the evaporated ones. This makes possible the use of very small electrodes in impedance measurement applications without the necessity of electrodeposition of other material to increase the active area and reduce the impedance.

The method used for sensing pH was the electrodeposition of iridium oxide film by electrochemical growth (AEIROF) onto the printed Pt electrodes. Sensors exhibited an excellent linear response in a wide range of pH (from 1 to 13) with high sensitivities and with fast response time ($<$ 1 second), when working with an external reference electrode. This study also integrates an Ag/AgCl printed pRE. The printed pRE exhibits a good performance, with a small drift of 0.4 mV/h. However, the use of the pRE limits the pH measured range, between 3 and 10.

All the results described above makes the presented manufacturing approach interesting for a wide range of sensor applications. The micrometric dimensions of the presented printed sensors allow their used in applications that requires disposable devices, low analysis time, sample volumes and portability for in-situ analysis. All these characteristics make this pH sensor of interest specially in the biomedical applications field.

This work demonstrates the well behavior of the AEIROF Pt printed electrodes. However, due to the lack of time in this Master Thesis, a lot of work must still be done. So, in order to complete the pH sensor characterization, an increased number of devices must be further test in order to obtain the LOQ/LOD, deviation, reproducibility and repeatability.

Further, in the future the GAB plans to improve this sensor trying to deposit by Inkjet printing a H+ sensible layer. This can be possible printing wiht a novel formulation of polypyrrole ink. In this way, and in the case that will be achieved, this would be the first full printed pH sensor device described in the literature.

Bibliography

[1] Guimera X, Moya A, Dorado AD, Villa R, Gabriel D, Gabriel G, Gamisans X Biofilm dynamics characterization using a novel DO-MEA sensor: mass transport and biokinetics Applied Microbiology and Biotechnology 99 (2015) 55-66

[2] Montero L, Gabriel G, Guimerà G, Villa R, Gleason KK, Borrós S. Increasing biosensor response through hydrogel thin film deposition: Influence of hydrogel thickness Vaccum 86 (2012) 2102-2104

[3] Prats-Alfonso E, Abad L, Casañ-Pastor N, Gonzalo-Ruiz J, Baldrich E Iridium oxide pH sensor for biomedical applications. Case urea-urease in real urine samples Biosensensors and Bioelectronics 39 (2013) 163-169

[4] P. L. Hue, J. Imaging Sci. Technol., 1998, 42, 49–62.

[5] 2 L. Rayleigh, Proc. London Math. Soc., 1878, s1–10, 4–13.

[6] P. W. Cooley, D. B. Wallace and B. V. Antohe, Applications of ink-jet printing technology to BioMEMS and microfluidic systems, San Francisco, CA, 2001.

[7] H. Kobayashi, N. Koumura and S. Ohno, Liquid recording medium. Assignee: Canon Kabushiki Kaisha, US4243994 A, 1981.

[8] S. Zoltan, Pulsed droplet ejecting system. Assignee: Gould Inc., US3857049 A, 1974.

[9] Fujifilm, User Manual DMP-2800 series, Doc. PM000040 Rev. 05, 2010.

[10] B.-J. de Gans, P.C. Duineveld, U.S. Schubert, Inkjet printing of polymers: stateof the art and future developments, Adv. Mater. 16 (3) (2004) 203–213.

[11] S. K. Volkman, S. Yin, T. Bakhishev, K. Puntambekar, V. Subramanian, and M. F. Toney, "Mechanistic studies on sintering of silver nanoparticles," Chem. Mater., vol. 23, no. 20, pp. 4634– 4640, 2011.

[12] H. C. Inc, “Harima Silver Nanopaste (NPS-J) Datasheet,” Japan.

[13] D. Huang, F. Liao, S. Molesa, D. Redinger, and V. Subramanian, “Plastic-compatible low resistance printable gold nanoparticle conductors for flexible electronics,” J. Electrochem. Soc., vol. 150, no. 7, pp. G412–G417, 2003.

[14] Nichols, Chem. Engr. Prog., 90(12), 64, 1994; McMillan, Chem. Engr. Prog., 87(12), 30, 1991

[15] Schwarzenbach, Gerold; Irving, Harry (tr.) (1957). Complexometric Titrations (1st English ed.). London: Methuen and Co. pp. 29–46.

[16] Perry, R H., and Don, W G. Perry’s Chemical Engineers’ Handbook. New York: McGraw-Hill, 2008.

[17] K. Pasztor, A. Sekiguchi, N. Shimo, N. Kitamura, H. Masuhara, Iridium oxidebased microelectrochemical transistors for pH sensing, Sensors and Actuators B 12 (1993) 225–230.

[18] O.S. Wolfbeis, Fiber-optic chemical sensors and biosensors, Analytical Chemistry 76 (2004) 3269–3284.

[19] G. Gerlach, M. Guenther, J. Sorber, G. Suchaneck, K.F. Arndt, A. Richter, Chemical and pH sensors based on the swelling behavior of hydrogels, Sensors and Actuators B 111 (2005) 555–561.

[20] P.J. Kinlen, J.E. Heider, D.E. Hubbard, A solid-state pH sensor based on a Nafioncoated iridium oxide indicator electrode and a polymer-based silver chloride reference electrode, Sensors and Actuators B 22 (1994) 13–25.

[21] Huang, W. -D, et al. ”A Flexible pH Sensor Based on the Iridium Oxide Sensing Film.” Sensors and Actuators, A: Physical 169.1 (2011): 1-11. SCOPUS. Web. 10 June 2016.

[22] M. Singh, H.M. Haverinen, P. Dhagat, G.E. Jabbour, Inkjet printing – process and its applications, Advanced Materials 22 (2010) 673–685.

[23] D. Tobjörk, H. Aarnio, P. Pulkkinen, R. Bollström, A. Määttänen, P. Ihalainen, T. Mäkelä, J. Peltonen, M. Toivakka, H. Tenhu, R. Österbacka, IR-sintering of ink-jet printed metal-nanoparticles on paper, Thin Solid Films 31 (2012) 2949–2955.

[24] A. Määttänen, P. Ihalainen, P. Pulkkinen, S. Wang, H. Tenhu, J. Peltonen, Inkjetprinted gold electrodes on paper: characterization and functionalization, ACS Applied Materials and Interfaces 4 (2012) 955–964.

[25] P. Ihalainen, H. Majumdar, A. Määttänen, S. Wang, R. Österbacka, J. Peltonen, Versatile characterization of thiol-functionalized printed metal electrodes on flexible substrates for cheap diagnostic applications, Biochimica et Biophysica Acta (BBA), in press. http://dx.doi.org/10.1016/j.bbagen.2012.09.007

[26] Y.H. Yun, B.K. Lee, J.S. Choi, S. Kim, B. Yoo, Y.S. Kim, K. Park, Y.W. Cho, A glucose sensor fabricated by piezoelectric inkjet printing of conducting polymers and bienzymes, Analytical Sciences 27 (2011) 375–379.

[27] Groza JR (1999) Nanosintering. NANOSTRUCTURED MATERIALS 12: 987–992.

[28] Van der Pauw, L. J. "A Method of Measuring Specific Resistivity and Hall Effect of Discs of Arbitrary Shape." Philips Research Reports 12.1 (1958): 1-9. Print.

[29] L. M. Fischer, M. Tenje, A. R. Heiskanen, N. Masuda, J. Castillo, A. Bentien, J. Émneus, M. H. Jakobsen, A. Boisen,. Gold cleaning methods for electrochemical detection applications. Microelectron. Eng. 2009, 86, 1282.

[30] J. Kang, P.A. Rowntree, Langmuir 23 (2007) 509.

[31] L.D. Burke, E.J. O'Sullivan, Journal of Electroanalytical Chemistry 117 (1981) 155.

[32] W. Olthuis, M. Robben, P. Bergveld, M. Bos, W. Van der Linden, Sensors and Actuators B: Chemical 2 (1990) 247.

[33] R. Meyer, S. Cogan, T. Nguyen, R. Rauh, IEEE Transactions on Neural Systems and Rehabilitation Engineering 9 (2001) 2.

[34] J. Mozota, B. Conway, Electrochimica Acta 28 (1983) 1.

[35] Ives, D.J.G., Janz, G.J. Reference Electrodes, Theory and Practice. Academic Press Inc, New York. 1961

[36] Katsube, T., Lauks, I., Zemel, J.N., 1982. Sensors and Actuators 2 (4), 399–410. Kinoshita, E., Ingman, F., Edwall, G., Thulin, S., Glab, S., 1986. Talanta 33 (2), 125–134.

[37] Yao,S.,Wang,M.,Madou,M.,2001.JournalofTheElectrochemicalSociety148(4), H29–H36.

[38] Cruz,A.M.,Abad,L.,Carretero,N.M.,Moral Vico,J.,Fraxedas,J.,Lozano,P.,Subias, G., Padial, V., Carballo, M., Collazos-Castro, J., Casan Pastor, N., 2012. The Journal of Physical Chemistry C 116, 5155–5168.

[39] Juodkazyte, Benjaminas Sebeka, Ignas Valsiunas, Kestutis Juodkazis. Iridium anodic oxidation to Ir3 and Ir2 hydrous oxides. Electroanalysis. June 2005. 17(11):947-952.

[40] Koncki, R.; Mascini, M. Screen-printed ruthenium dioxide electrodes for pH measurements. Anal. Chim. Acta 1997, 351, 143–149.

[41] Muller, A.; Brinz,T.; Simon, U. Preparation and Measurement of Combinatorial Screen Printed Libraries for the Electrochemical Analysis of Liquids. J. Comb. Chem. 2008, 11, 138–142.

[42] Kampouris, Dimitrios K. and Kadara, Rashid O. and Jenkinson, Norman and Banks, Craig E., Screen printed electrochemical platforms for pH sensing, Volumen 1, 2009, Pages 25-28, http://dx.doi.org/10.1039/B9AY00025A.

[43] Cheng-En Lue, I-Shun Wang, Chi-Hsien Huang, Yu-Ting Shiao, Hau-Cheng Wang, Chia-Ming Yang, Shu-Hao Hsu, Ching-Yu Chang, William Wang, Chao-Sung Lai, pH sensing reliability of flexible ITO/PET electrodes on EGFETs prepared by a roll-to-roll process, Microelectronics Reliability, Volume 52, Issue 8, August 2012, Pages 1651-1654, ISSN 0026-2714, http://dx.doi.org/10.1016/j.microrel.2011.10.026.

[44] Yiheng Qin, Hyuck-Jin Kwon, Ayyagari Subrahmanyam, Matiar M.R. Howlader, P. Ravi Selvaganapathy, Alex Adronov, M. Jamal Deen, Inkjet-printed bifunctional carbon nanotubes for pH sensing, Materials Letters, Volume 176, 1 August 2016, Pages 68-70, ISSN 0167-577X, http://dx.doi.org/10.1016/j.matlet.2016.04.048.

[45] E. T. S. G da Silva, S. Miserere, L. T. Kubota, A. Merkoci, Anal. Chem. 2014, 86, 10531.

[46] Moya A, Zine N, Illa X, et al. Flexible Polyimide Platform based on the Integration of Potentiometric Multi-sensor for Biomedical Applications. Procedia Eng. 2014;87:276-279. doi:10.1016/j.proeng.2014.11.661.

[47] F. J. del Campo, L. Abad, X. Illa, E. Prats-Alfonso, X. Borrisé, J. M. Cirera, H.-Y. Bai, Y.-C. Tsai, Sens. Actuators B Chem. 2014, 194, 86.

[48] E. T. S. G. da Silva, S. Miserere, L. T. Kubota, A. Merkoçi, Anal. Chem. 2014, 86, 10531.

[49] ELisa Castagnola, Alberto Ansaldo, Emma Maggiolini, Tamara Ius, Miran Skrap, Davide Ricci, and Luciano Fadiga. Smaller, softer, lower-impedance electrodes for human neuroprosthesis: a pragmatic approach. Frontiers in neuroengineering, 7, 2014.

[50] Gemma Gabriel, Ivan Erill, Jaume Caro, Rodrigo Gómez, Dolors Riera, Rosa Villa, Philippe Godignon, Manufacturing and full characterization of silicon carbide-based multi-sensor microprobes for biomedical applications, Microelectronics Journal, Volume 38, Issue 3, March 2007, Pages 406-415, ISSN 0026-2692, http://dx.doi.org/10.1016/j.mejo.2006.11.008.

[51] A. J. Bard, L. R. Faulkner, Electrochemical methods: fundamentals and applications; Wiley: New York, 2001.

[52] P. T. Kissinger, W. R. Heineman, J. Chem. Educ. 1983, 60, 702.

[53] R. O. Kadara, N. Jenkinson, C. E. Banks, Sens. Actuators B Chem. 2009, 138, 556.

[54] G. Gabriel, X. Illa, A. Guimera, B. Rebollo, J. Hernández-Ferrer, M. Martinez, P Godignon, M. Sanchez-Vives, R. Villa. Carbon Nanotubes as Suitable Interface for Improving Neural Recordings. C 15. DOI: 10.5772/52174

[55] H. Matsuda, Y. Ayabe, Bull. Chem. Soc. Jpn. 1955, 28, 422.